HYDROGEN GAS SENSING AND STORAGE PROPERTIES OF DOPED AND NON-DOPED BERYLLIUM OXIDE NANOTUBES

Mr. Kritsanaphas Sawing

จุฬาลงกรณ์มหาวิทยาลัย
CHULALONGKORN UNIVERSITY

A Thesis Submitted in Partial Fulfillment of the Requirements
for the Degree of Master of Science in Chemistry
Department of Chemistry
FACULTY OF SCIENCE
Chulalongkorn University
Academic Year 2021
Copyright of Chulalongkorn University

สมบัติการรับรู้และกักเก็บแก๊สไฮโดรเจนของท่อนาโนเบริลเลียมออกไซด์ที่ถูกเจือและไม่ถูกเจือ

นายกฤษณภัสร์ สวิง

จุฬาลงกรณ์มหาวิทยาลัย
CHULALONGKORN UNIVERSITY

วิทยานิพนธ์นี้เป็นส่วนหนึ่งของการศึกษาตามหลักสูตรปริญญาวิทยาศาสตรมหาบัณฑิต
สาขาวิชาเคมี ภาควิชาเคมี
คณะวิทยาศาสตร์ จุฬาลงกรณ์มหาวิทยาลัย
ปีการศึกษา 2564
ลิขสิทธิ์ของจุฬาลงกรณ์มหาวิทยาลัย

Thesis Title	HYDROGEN GAS SENSING AND STORAGE PROPERTIES OF DOPED AND NON-DOPED BERYLLIUM OXIDE NANOTUBES
By	Mr. Kritsanaphas Sawing
Field of Study	Chemistry
Thesis Advisor	Professor VITHAYA RUANGPORNVISUTI, Dr.rer.nat.

Accepted by the FACULTY OF SCIENCE, Chulalongkorn University in Partial Fulfillment of the Requirement for the Master of Science

..... Dean of the FACULTY OF SCIENCE
(Professor POLKIT SANGVANICH, Ph.D.)

THESIS COMMITTEE

..... Chairman
(Professor VUDHICHAI PARASUK, Ph.D.)
..... Thesis Advisor
(Professor VITHAYA RUANGPORNVISUTI, Dr.rer.nat.)
..... Examiner
(Associate Professor VIWAT VCHIRAWONGKWIN, Dr.rer.nat.)
..... External Examiner
(Assistant Professor Banchob Wanno, Ph.D.)

จุฬาลงกรณ์มหาวิทยาลัย
Chulalongkorn University

กฤษณภัสร์ สวิง : สมบัติการรับรู้และกักเก็บแก๊สไฮโดรเจนของท่อนาโนเบริลเลียมออกไซด์ที่ถูกเจือและไม่ถูกเจือ. (HYDROGEN GAS SENSING AND STORAGE PROPERTIES OF DOPED AND NON-DOPED BERYLLIUM OXIDE NANOTUBES)
อ.ที่ปรึกษาหลัก : ศ. ดร.วิทยา เรืองพรวิสุทธิ์

การศึกษาสมบัติทางอิเล็กทรอนิกส์ของท่อนาโนเบริลเลียมออกไซด์ (BeONT) ที่มีโครงสร้างอาร์มแชร์ (5,5) และโครงสร้างซิกแซก (10,0) ที่ไม่ถูกเจือและถูกเจือด้วยธาตุคาบที่ 2 (โบรอน คาร์บอน และเจอร์เมเนียม), 3 (แมกนีเซียม อะลูมิเนียม ซิลิกอน ฟอสฟอรัส และซัลเฟอร์) และ4 (แคลเซียม แกลเลียม เจอร์เมเนียม อาร์เซนิก และเซเลเนียม) ได้รับการศึกษาโดยวิธีพีริออดิก ดีเอฟทีดี พบว่าโครงสร้างท่อนาโนเบริลเลียมออกไซด์แบบอาร์มแชร์ที่เจือด้วยคาร์บอน และเจอร์เมเนียม ที่ตำแหน่งออกซิเจน และแบบซิกแซกที่ถูกเจือด้วยคาร์บอน ซิลิกอน และเจอร์เมเนียม ที่ตำแหน่งออกซิเจนจน สามารถเป็นวัสดุตรวจจับแก๊สไฮโดรเจน เนื่องจากช่องว่างพลังงานเปลี่ยนแปลงมาก ในขณะที่โครงสร้างแบบอาร์มแชร์ที่เจือด้วยคาร์บอน ซิลิกอน และเจอร์เมเนียม ที่ตำแหน่งออกซิเจน และแบบซิกแซกที่ถูกเจือด้วยคาร์บอน ซิลิกอน ที่ตำแหน่งออกซิเจน สามารถเป็นตัวกักเก็บแก๊สไฮโดรเจนที่ เนื่องจากดูดซับแก๊สไฮโดรเจนได้ดี

จุฬาลงกรณ์มหาวิทยาลัย
Chulalongkorn University

สาขาวิชา เคมี ลายมือชื่อนิสิต .....

ปีการศึกษา 2564 ลายมือชื่อ อ.ที่ปรึกษาหลัก .....

6172017323 : MAJOR CHEMISTRY
KEYWORD: periodic DFT–D, doped, hydrogen molecule adsorptions, beryllium oxide nanotube, BeONT

Kritsanaphas Sawing : HYDROGEN GAS SENSING AND STORAGE PROPERTIES OF DOPED AND NON-DOPED BERYLLIUM OXIDE NANOTUBES. Advisor: Prof. VITHAYA RUANGPORNVISUTI, Dr.rer.nat.

The electronic properties of armchair (5,5) beryllium oxide nanotube (BeONT), zigzag (10,0) BeONT, and their surfaces doped by the selected elements of periods 2 (B, C and N), 3 (Mg, Al, Si, P and S) and 4 (Ca, Ga, Ge, As and Se), and their hydrogen molecule adsorptions were studied using periodic DFT–D method. The $C^{(O)}$– and $Ge^{(O)}$–(5,5) BeONTs, $C^{(O)}$–, $Si^{(O)}$– and $Ge^{(O)}$–(10,0) BeONTs were suggested to be new hydrogen molecule sensing materials based on the electrical resistivity measurement. The $C^{(O)}$–, $Si^{(O)}$– and $Ge^{(O)}$–doped (5,5) BeONTs, and $C^{(O)}$– and $Si^{(O)}$–doped (10,0) BeONTs were suggested to be utilized as hydrogen storage materials.

จุฬาลงกรณ์มหาวิทยาลัย
CHULALONGKORN UNIVERSITY

Field of Study:	Chemistry	Student's Signature .....
Academic Year:	2021	Advisor's Signature .....

ACKNOWLEDGEMENTS

First of all, I would like to express my sincere gratitude to Professor Vithaya Ruangpornvisuti, my research advisor, for his guidance, constructive suggestion, plentiful experience, understanding, encouragement, and supporting me throught the course of this research.

Furthermore, I would like to thank my Thesis committee members: Professor Vudhichai Parasuk, Associate Professor Viwat Vchirawongkwin, and Assistant Professor Banchob Wanno for their advice and insightful comment.

Then, Special thank to VR lab members for their help and suggestion. I would like to thank my friend and Kemes student for all their good supporting and friendship.

Finally, I would like to thank my mother and sister for supporting, trusting and believing in my decisions. I am so proud of them.

Kritsanaphas Sawing

จุฬาลงกรณ์มหาวิทยาลัย
Chulalongkorn University

TABLE OF CONTENTS

Page

ABSTRACT (THAI) iii
ABSTRACT (ENGLISH) iv
ACKNOWLEDGEMENTS v
TABLE OF CONTENTS vi
LIST OF TABLES viii
LIST OF FIGURES ix
CHAPTER I INTRODUCTION 1
1.1 Background 1
1.2 Beryllium oxide nanotube 4
1.3 Objective 5
CHAPTER II THEORETICAL BACKGROUND 6
2.1 Density functional theory (DFT) method 6
2.1.1 Density functional theory 6
2.1.2 The Kohn-Sham equations 8
2.1.3 Basis set 10
2.1.4 Effective core pseudopotential (ECP) 11
2.2 Dispersion-corrected density functional theory (D-DFT) method 12
CHAPTER III MODELS AND METHODS 13
3.1 Computational method 13
CHAPTER IV RESULTS AND DISCUSSIONS 17
4.1 Adsorption on (5,5) BeONT and its doping derivatives 17
4.1.1 The structures of the pristine (5,5) BeONT and periods 2–4 elements doped (5,5) BeONT surfaces 17
4.1.2 Adsorption of the hydrogen molecule on the pristine (5,5) BeONT and periods 2–4 elements–doped (5,5) BeONT surfaces 23
4.1.2.1 Period 2 elements 24

จุฬาลงกรณ์มหาวิทยาลัย
Chulalongkorn University

4.1.2.2 Period 3 elements 26
4.1.2.3 Period 4 elements 28
4.1.3 Energy gaps of pristine and periods 2–4 elements–doped (5,5) BeONTs, and their hydrogen adsorption complexes 31
4.2 Adsorption on (10,0) BeONT and its doping derivatives 36
4.2.1 The structures of the pristine (10,0) BeONT and periods 2–4 elements–doped (10,0) BeONT surfaces 36
4.2.2 Adsorption of the hydrogen molecule on the pristine (10,0) BeONT and periods 2–4 elements–doped (10,0) BeONT surfaces 41
4.2.2.1 Period 2 elements 42
4.2.2.2 Period 3 elements 44
4.2.2.3 Period 4 elements 46
4.2.3 Energy gaps of pristine and periods 2–4 elements–doped (10,0) BeONTs, and their hydrogen adsorption complexes 49
4.3 Hydrogen absorption and sensing abilities of M-BeONTs comparing with other nanotubes in literature 54
CHAPTER V CONCLUSION 56
REFERENCES 59
VITA 65

จุฬาลงกรณ์มหาวิทยาลัย
Chulalongkorn University

LIST OF TABLES

Page

Table 4.1 Energy gaps (E_g) and energy–gap changes of H_2 adsorption on the pristine and M–doped (5,5) BeONTs and their doping energies 32

Table 4.2 Adsorption energies (ΔE_{ads}) of H_2 adsorption on the pristine and M–doped (5,5) BeONTs.....33

Table 4.3 Mülliken–charges (in e) of selected atoms on the M–doped (5,5) BeONTs, their H_2 adsorption complexes and changes of their charges (Δq). 34

Table 4.4 Energy gaps (E_g) and energy–gap changes of H_2 adsorption on the pristine and M–doped (10,0) BeONTs and their doping energies 50

Table 4.5 Adsorption energies (ΔE_{ads}) of H_2 adsorption on the pristine and M–doped (10,0) BeONTs.....51

Table 4.6 Mülliken–charges (in e) of selected atoms on the M–doped (10,0) BeONTs, their H_2 adsorption complexes, and changes of their charges (Δq). 52

จุฬาลงกรณ์มหาวิทยาลัย
CHULALONGKORN UNIVERSITY

LIST OF FIGURES

Page

Figure 1.1 The structures of (a) the 3D wurzite-like BeO, (b) the h-BeO monolayer and (c) the (10,0) BeO nanotube [41]. 4

Figure 1.2 Top and side views of atomic structures of single-walled: 1.- zigzag (10,0) and 2- armchair (6,6) nanotubes of graphite-like hexagonal BeO [47]. 5

Figure 4.1 Optimized structure of the pristine (5,5) BeONT. Left and right are two different side views and front views, respectively. 18

Figure 4.2 Optimized structures of the (a) B–, (b) $C^{(Be)}$ –, (c) $C^{(O)}$ – and (d) N–doped (5,5) BeONTs. Left and right images are side and front views, respectively. 19

Figure 4.3 Optimized structures of the (a) Mg–, (b) Al–, (c) $Si^{(Be)}$ –, (d) $Si^{(O)}$–, (e) P– and (f) S–doped (5,5) BeONTs. Left and right images are side and front views, respectively. 20

Figure 4.4 Optimized structures of the (a) Ca–, (b) Ga–, (c) $Ge^{(Be)}$ –, (d) $Ge^{(O)}$–, (e) As–and (f) Se–doped (5,5) BeONTs. Left and right images are side and front views, respectively. 21

Figure 4.5 Plots of doping energy of the (5,5) BeONT doped by the (a) period 2, (b) period 3 and (c) period 4 element. Their upper and lower curves are of the doping on the O and Be vacancies in the (5,5) BeONT, respectively. 22

Figure 4.6 Adsorption structure of H_2 adsorbed on the pristine (5,5) BeONT. Left and right are two different side views and front views, respectively. 23

Figure 4.7 Adsorption structures of H_2 adsorbed on the (a) B–, (b) $C^{(Be)}$ –, (c) $C^{(O)}$ – and (d) N–doped (5,5) BeONTs. Left and right images are side and front views, respectively. 25

Figure 4.8 Adsorption structures of H_2 adsorbed on the (a) Mg–, (b) Al–, (c) $Si^{(Be)}$ –, (d) $Si^{(O)}$ –, (e) P– and (f) S–doped (5,5) BeONTs. Left and right images are side and front views, respectively. 27

Figure 4.9 Adsorption structures of H_2 adsorbed on the (a) Ca–, (b) Ga–, (c) $Ge^{(Be)}$ –, (d) $Ge^{(O)}$ –, (e) As– and (f) Se–doped (5,5) BeONTs. Left and right images are side and front views, respectively. 29

Figure 4.10 Plots of adsorption energy of hydrogen molecule on the (5,5) BeONT doped by elements of the (a) period 2, (b) period 3, and (c) period 4. The adsorptions of hydrogen molecules on the $C^{(Be)}$, $Si^{(Be)}$, and $Ge^{(Be)}$ are by the red circle. 30

CHULALONGKORN UNIVERSITY

Figure 4.11 Optimized structures of the pristine (10,0) BeONTs. Left and right images are two different side and front views, respectively. 37

Figure 4.12 Optimized structures of the (a) B–, (b) $C^{(Be)}$–, (c) $C^{(O)}$– and (d) N–doped (10,0) BeONTs. Left and right images are side and front views, respectively. 38

Figure 4.13 Optimized structures of the (a) Mg–, (b) Al–, (c) $Si^{(Be)}$–, (d) $Si^{(O)}$–, (e) P– and (f) S–doped (10,0) BeONTs. Left and right images are side and front views, respectively. 38

Figure 4.14 Optimized structures of the (a) Ca–, (b) Ga–, (c) $Ge^{(Be)}$–, (d) $Ge^{(O)}$–, (e) As–and (f) Se–doped (10,0) BeONTs. Left and right images are side and front views, respectively. 39

Figure 4.15 Plots of doping energy of the (10,0) BeONT doped by elements of the (a) period 2, (b) period 3, and (c) period 4. Their upper and lower curves are of the doping on the O and Be vacancies of the (10,0) BeONT, respectively. 40

Figure 4.16 Adsorption structures of H_2 adsorbed on the pristine (10,0) BeONTs. Left and right images are side and front views, respectively. 41

Figure 4.17 Adsorption structures of H_2 adsorbed on the (a) B–, (b) $C^{(Be)}$–, (c) $C^{(O)}$– and (d) N–doped (10,0) BeONTs. Left and right images are side and front views, respectively. 43

Figure 4.18 Adsorption structures of H_2 adsorbed on the (a) Mg–, (b) Al–, (c) $Si^{(Be)}$–, (d) $Si^{(O)}$–, (e) P–and (f) S–doped (10,0) BeONTs. Left and right images are side and front views, respectively. 45

Figure 4.19 Adsorption structures of H_2 adsorbed on the (a) Ca–, (b) Ga–, (c) $Ge^{(Be)}$–, (d) $Ge^{(O)}$–, (e) As–and (f) Se–doped (10,0) BeONTs. Left and right images are side and front views, respectively. 47

Figure 4.20 Plots of adsorption energy of hydrogen molecule on the (10,0) BeONT doped by elements of the (a) period 2, (b) period 3, and (c) period 4. The adsorptions of hydrogen molecules on the $C^{(Be)}$, $Si^{(Be)}$, and $Ge^{(Be)}$ are by the red circle. 48

จุฬาลงกรณ์มหาวิทยาลัย
Chulalongkorn University

CHAPTER I
INTRODUCTION

1.1 Background

Since the single-walled carbon nanotube (SWCNT) which consists hexagonal rings of carbon atoms, was discovered[1], hydrogen adsorptions on pristine, defect SWCNTs and their derivatives as Eu- , Ce- and Na-doped , and Ti- and Pt-decorated SWCNTs were studied for their hydrogen storage properties[2-10]. Explorations for hydrogen storage materials, the adsorption of hydrogen molecule on the boron nitride nanotubes (BNNTs)[11-17], defective , C-, Pt-, Al-doped and Ce-doped, Rh-, Ni- and Pd-functionalized and Pt- and Ti-decorated BNNTs were investigated[18-25]. The physisorption of hydrogen molecule on BNNT was found to be favorable energetically than on the SWCNT[17]. The dissociative adsorption of the hydrogen molecule on the perfect and the Stone-Wales defects BNNTs were found[18]. The hydrogen adsorbed on the top of the C atom of the C-doped BNNT was found[19]. One and two hydrogen molecules were found to be chemically adsorbed on the Pt-doped BNNT and the single Pt decorated BNNT, respectively[20]. The hydrogen adsorption on the Al-doped zigzag and armchair BNNTs was investigated and their potential capacity to adsorb hydrogen was found[21]. The seven hydrogen molecules per Ce atom of the Ce-doped BNNT and 5.68 wt% H_2 stored in the Ce3/BNNT system were indicated[22]. The hydrogen capacities for Rh-, Ni- and Pd-functionalized BNNTs as efficient hydrogen storage were predicted[23]. The hydrogen molecule physisorption occurring near the Ti atom of the Ti-decorated BNNTs was observed, and their storage capacity for hydrogen molecules was suggested[24]. The seven H_2 molecules physisorbed at the vicinity of the Ti atom of the Ti-decorated BNNTs were revealed by MD simulation[25], and Ti-decorated (10,0) BNNTs with B–N defects were examined by the DFT and molecular dynamics (MD) simulation[26].

As the BNNT, well-known non-carbon nanotube (inorganic carbon nanotube), and its derivatives have been attended as hydrogen storage materials, the adsorption

of hydrogen molecule on the beryllium oxide nanotube (BeONT) and its derivatives should, therefore, be fascinatingly explored. Lead to the BeONTs are isoelectronic to SWCNTs and BNNTs and exhibit the increased polarity of the bond, the structures and electronic properties of BeONTs as new non-carbon nanotube were theoretically predicted[27]. The structural, elastic, and electronic properties of various sizes of zigzag and armchair BeONTs were studied by DFT compared with the BNNTs[28]. The electronic structure and magnetism in pristine (6,6) and (10,0) BeONTs were studied using DFT computations compared with the B-, C-, and N-doped (6,6) and (10,0) BeONTs[29]. The electronic structures, optical absorption spectra, the modulation of uniaxial strain along tube axis to electronic structures and optical absorption spectra[30], electronic and linear optical properties[31] of BeONTs were investigated by the DFT method. The structural, electronic, and magnetic properties of BeONTs and 3d transition metal-doped BeONTs and the structural, electrical, and optical properties of pristine and B-, Al-, Ga-doped BeONTs were studied[32, 33]. Dilute magnetic semiconductor and half-metal behaviors in C-co doped BeONTs were studied[34]. The electronic and field emission characteristics of (5, 5) capped BeONTs were studied[35]. The adsorption H_2S molecule on the pristine and Si-doped BeONT[36], aniline electrical sensing of BeONT[37], nitrous oxide on pristine and defective BeONTs[38], CO_2 molecule on BeONT[39], and adenine on BeONT[40] were investigated using DFT methods. It was shown that BeONTs are thermodynamically stable and have binding energy close to the binding energy observed for beryllium oxide with a wurtzite structure. The structural, elastic, and electronic properties of the BeONT were studied compared with BNNT[41]. The zigzag BeONTs of the (n,0), where n = 8 to 64, were simulated and the properties were studied by periodic DFT method. The electronic and the linear optical properties of the BeONTs were investigated[31]. The electronic structures and absorption spectra of the BeONTs were studied and the armchair BeONTs were suggested to be used as the sensor of photoelectron and anisotropic device[42]. The optical absorption frequency behavior of the BeONT was studied and compared with BNNT[43]. The structural, electrical, linear, and nonlinear optical (NLO) properties of the pristine and B, Al, and Ga doped BeONTs were studied by DFT method[44].

จุฬาลงกรณ์มหาวิทยาลัย
Chulalongkorn University

Electronic structure and magnetism of the pristine, B-, C-, and N-doped BeONTs were studied[45-47]. Effects of the 3d transition metal doping on the structural, electronic, and magnetic properties of BeONTs were studied and the V-, Co-, and Ni-doped (5,5) and (8,0) BeONTs with half-metal ferromagnetism and 100% spin polarization character were suggested as good candidates for spintronic applications[48]. Nevertheless, research for exploration of hydrogen adsorption on BeONTs and their doping derivatives for hydrogen storage and/or sensing materials has hardly been found. The beryllium oxide nano-cage (BeONC), the small size ($Be_{12}O_{12}$), was studied on its hydrogen adsorption and the average adsorption energy of −0.11eV was obtained[49].

จุฬาลงกรณ์มหาวิทยาลัย
Chulalongkorn University

1.2 Beryllium oxide nanotube

Beryllium oxide (BeO) is a transitional material between ionic compound and semiconductive material for example BN and ZnO[50, 51]. On the contrary alkaline earth oxides, crystalline BeO which is a compact wurtzite structure, is an insulator in electronics (band gap ~10 eV) with very high thermal conductivity, high melting point and elastic[52]. Moreover, Beryllium oxide nanotubes (BeONTs) which are constructed by rolled up a BeO sheet, can be divided into 3 types : armchair nanotubes (n=m), zigzag nanotubes (n≠0, m=0) and chiral nanotubes (n≠m) were found that band gap have 7.3-8.8 eV which depend on chirality and diameter[27, 41, 53].

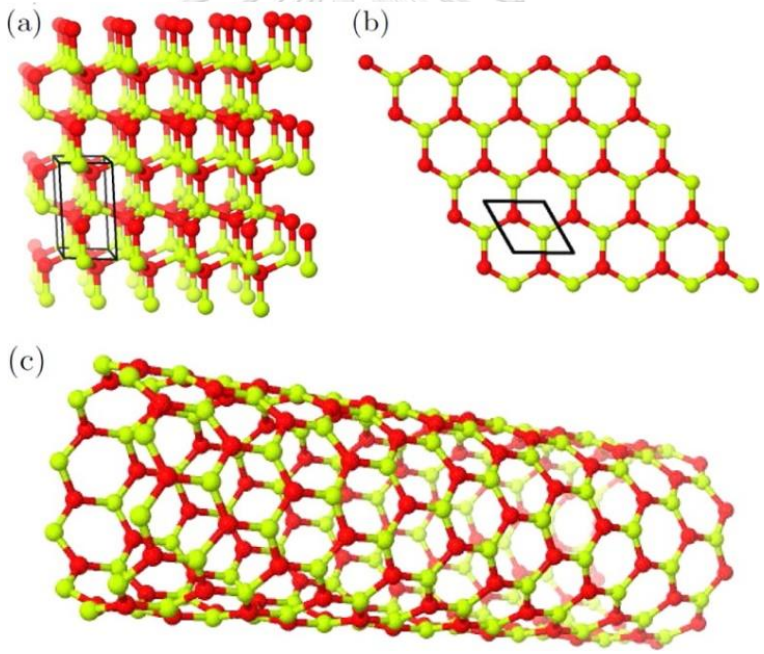

Figure 1.1 The structures of (a) the 3D wurzite-like BeO, (b) the h-BeO monolayer and (c) the (10,0) BeO nanotube [41].

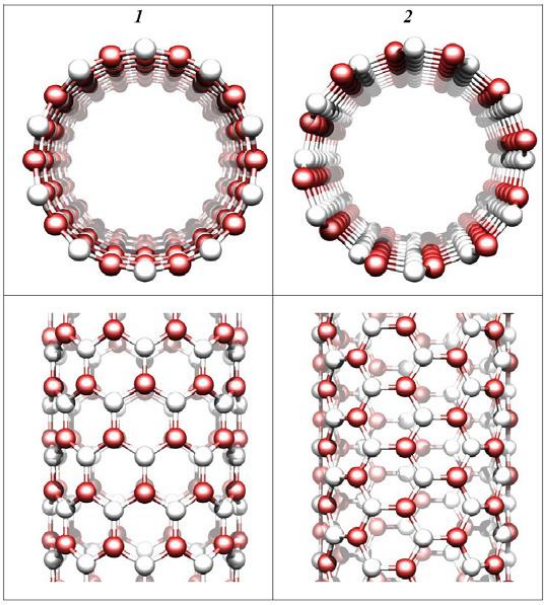

Figure 1.2 Top and side views of atomic structures of single-walled: 1.- zigzag (10,0) and 2- armchair (6,6) nanotubes of graphite-like hexagonal BeO [47].

1.3 Objective

In this work, we employed periodic DFT-D calculations to investigate the (5,5) and (10,0) BeONTs, and their surfaces doped by selected elements of periods 2 (B, C, and N), 3 (Mg, Al, Si, P, and S) and 4 (Ca, Ga, Ge, As and Se), and doping processes of all the element doped BeONTs. In addition, the adsorption of hydrogen molecules on all the studied surfaces was explored to discover new hydrogen storage and hydrogen sensing materials.

จุฬาลงกรณ์มหาวิทยาลัย
Chulalongkorn University

CHAPTER II
THEORETICAL BACKGROUND

There are three tools used to investigate the chemical properties of atoms, molecules and solids consisting of semi-empirical, Hartree-Fock (HF) and density functional theory (DFT) methods. DFT is a most popular method that was continuously developed to be used for calculations in this Thesis.

2.1 Density functional theory (DFT) method

Density functional theory (DFT) is a Quantum Mechanic (QM) method in the study the electronic structure of atoms, molecules and solids. DFT is based on the total electronic charge density $\rho(\mathbf{r})$, which is more directly related to observable quantities than is the N-electron wave function $\psi(\mathbf{r}_1,\mathbf{r}_2...\mathbf{r}_N)$. The density function determine from the wave function using

$$\rho(\mathbf{r}) = N \iint \cdots \int |\psi(\mathbf{r},\mathbf{r}_2 \ldots \mathbf{r}_N)|^2 \, ds dx_2 \ldots dx_N \qquad (2.1)$$

where $\mathbf{r}_1$ has been singled out for replacement by the unlabeled three-dimensional variable $\mathbf{r}$. Note that integration runs over space and spin coordinates of electrons 2,3...N, but only over the spin of the first electron [54].

จุฬาลงกรณ์มหาวิทยาลัย
Chulalongkorn University

2.1.1 Density functional theory

The fundamental quantity is the energy considered as a functional of the electron density: $E[\rho]$. This is conveniently divided into four contributions:

$$E[\rho] = E_K[\rho] + E_V[\rho] + E_J[\rho] + E_{XC}[\rho] \qquad (2.2)$$

An exact form for the kinetic energy functional is not known but, as a first approximation,

$$E_K[\rho] = \frac{3}{10}(3\pi^2)^{\frac{2}{3}} \int \rho(\mathbf{r})^{\frac{5}{3}} \mathrm{d}^3\mathbf{r} \tag{2.3}$$

which is suggested by the local density approximation used in the Thomas-Fermi atomic model. A correction to $E_K[\rho]$ which considers also the gradient of the density is the *Weizsacker* correction:

$$\Delta E_K^W[\rho] = \frac{\lambda}{8} \int \frac{|\nabla\rho(\mathbf{r})|^2}{\rho(\mathbf{r})} d^3\mathbf{r} \tag{2.4}$$

where λ is an empirical constant. The potential energy of nuclear-electronic and internuclear interactions in a molecule is given by

$$E_V[\rho] = -\sum_A Z_A \int \frac{\rho(\mathbf{r})}{|\mathbf{r}-\mathbf{R}_A|} d^3\mathbf{r} + \sum_{A<B} \frac{Z_A Z_B}{R_{AB}} \tag{2.5}$$

จุฬาลงกรณ์มหาวิทยาลัย
Chulalongkorn University

where the electron-electron potential energy is

$$E_J[\rho] = \frac{1}{2} \iint \frac{\rho(\mathbf{r}_1)\rho(\mathbf{r}_2)}{r_{12}} \mathrm{d}^3\mathbf{r}_1 \mathrm{d}^3\mathbf{r}_2 \tag{2.6}$$

This has to be corrected by subtracting out electron self-interactions, which is done by the exchange potential. Both potential-energy parts have analogs in classical electromagnetic theory. The exchange-correlation functional is the most challenging. It is entirely of quantum-mechanical origin the Pauli exclusion principle and electron correlation. An early approximation to the exchange part of this contribution, introduced by Slater to be discussed in the following section.

$$E_X[\rho] = -\frac{3\alpha}{2}\left(\frac{3}{\pi}\right)^{\frac{1}{3}} \int \rho(\mathbf{r})^{\frac{4}{3}} d^3\mathbf{r} \tag{2.7}$$

where α is another empirical constant.

The Lieb-Oxford bound provides an upper limit to the exact exchange-correlation energy, namely

$$E_{XC}[\rho] \geq -1.68 \int \rho(\mathbf{r})^{\frac{4}{3}} d^3\mathbf{r} \tag{2.8}$$

By further manipulation of both functional forms and empirical parameters, which we will not describe in detail, a very successful formulation of DFT has been realized.

2.1.2 The Kohn-Sham equations

Kohn and Sham (1965) developed an alternative computational scheme which is a hybrid between DFT and the Hartree-Fock method. In particular, the complicated many-electron potential in the Hartree-Fock equation for a spin orbital is replaced by an effective potential $V_{\mathrm{KS}}(\mathbf{r})$ incorporating Coulomb, exchange and correlation effects. The actual many-electron system is thereby represented by an equivalent system with independent particles, such that a single Slater determinant gives the exact solution. A major advantage of the KS method is that it is no longer necessary to approximate the kinetic energy by local density type approximations. The kinetic energy of a spin orbital is now represented by the correct quantum mechanical operator $-\frac{\hbar^2}{2m}\nabla^2$. The Hartree-Fock-Kohn-Sham equation for a spin orbital $\phi_{\mathrm{n}}(\mathbf{r})$ (in atomic units) can be written

$$\left\{-\frac{1}{2}\nabla^2 + V_{\mathrm{KS}}(\mathbf{r})\right\}\phi_n(\mathbf{r}) = \epsilon_n\phi_n(\mathbf{r}) \tag{2.9}$$

จุฬาลงกรณ์มหาวิทยาลัย
Chulalongkorn University

where

$$V_{\mathrm{KS}}(\mathbf{r}) = -\sum_{A} \frac{Z_A}{|\mathbf{r}-\mathbf{R}_A|} + V_J[\rho] + V_{XC}[\rho] \tag{2.10}$$

The last functional includes correlation (absent in HF) as well as exchange.

A quite successful empirical approximation to the exchange-correlation potential was found by Gunnarsson and Lundqvist (1976)

$$V_{XC}[\rho] = -\frac{0.458}{r_s} - 0.0666 G\left(\frac{r_s}{11.4}\right) \tag{2.11}$$

where

$$\mathrm{G}(x) = \frac{1}{2}\left[(1+x^3)\log(1+x^{-1}) - x^2 + \frac{x}{2} - \frac{1}{3}\right] \tag{2.12}$$

Here, r_s is the Wigner-Seitz radius,

จุฬาลงกรณ์มหาวิทยาลัย
CHULALONGKORN UNIVERSITY

$$r_s = \left(\frac{3}{4\pi|\rho(\mathbf{r})|}\right)^{\frac{1}{3}} \tag{2.13}$$

the radius of a spherical volume containing an average of one electron.

At each stage of an iterative computation, the density is calculated using

$$\rho(\mathbf{r}) = \sum_{a} |\psi_a(\boldsymbol{r})|^2 \tag{2.14}$$

The exchange-correlation potential is formally related to the exchange-correlation energy in by a *functional derivative*

$$V^{XC}[\rho] = \frac{\delta E^{XC}[\rho]}{\delta \rho} \equiv \lim_{\Delta\rho \to 0} \frac{E^{XC}[\rho + \Delta\rho] - E^{XC}[\rho]}{\Delta\rho} \tag{2.15}$$

2.1.3 Basis set

Basis set is a set of mathematical basis functions representing the molecular orbitals. Linear combination of functions including the weights or coefficients describes molecular orbitals. It is composed of finite number of atomic orbitals within the system. This approximated molecular orbital is called LCAO approach. Moreover, the basis functions are described by the electron distribution around atom in the system.

CRYSTAL performs ab initio calculations on periodic systems within the linear combination of atomic orbitals (LCAO) approximation. The crystalline orbitals (CO) are treated as linear combinations of Bloch functions (BF) [55],

$$\psi_i(\mathbf{r};\mathbf{k}) = \sum_{\mu} a_{\mu,i}(\mathbf{k}) \phi_{\mu}(\mathbf{r};\mathbf{k}) \tag{2.16}$$

จุฬาลงกรณ์มหาวิทยาลัย
Chulalongkorn University

$$\phi_{\mu}(\mathbf{r};\mathbf{k}) = \sum_{\mathbf{g}} \psi_{\mu}(\mathbf{r} - \mathbf{A}_{\mu} - \mathbf{g}) e^{i\mathbf{k}\cdot\mathbf{g}} \tag{2.17}$$

This is defined in terms of local functions, hereafter indicated as atomic orbitals (AO). Those local functions are expressed as linear combination of a certain number of Gaussian type functions (GTF).

$$\psi_{\mu}(\mathbf{r} - \mathbf{A}_{\mu} - \mathbf{g}) = \sum_{j}^{n_G} d_j G(\alpha_j; \mathbf{r} - \mathbf{A}_{\mu} - \mathbf{g}) \tag{2.18}$$

where **r** is coordinate of an electron. **g** is direct lattice vector the sum over **g** is extended to the all-lattice vector(infinite) of direct lattice. **k** is lattice vector defining a point in the reciprocal lattice. **A** is coordinated of an atom in the reference cell. **a** is variational coefficients. **d** is coefficients of the primitive gaussians in the contraction, fixed for a given basis set; the sum over *j* is limited to the number of functions in the contraction.

The AOs belonging to a given atom are grouped into shells. The shell can contain either all AOs with the same quantum numbers, n and l (for instance 3s, 2p, 3d shells), or all the AOs with the same principal quantum number n and different l (sp shells; exponent of s and p gaussians are the same). A single, normalized, s-type GTF, the adjoined gaussian, is associated with each shell. The exponent of the adjoined gaussian is the smallest exponent of the gaussians in the contraction. The adjoined gaussian is used to estimate the AO overlap and select the level of approximation to be adopted for the evaluation of the integrals.

The basis set definition is the first step to uniquely define the level of calculation. The molecular and crystalline basis set must be balanced, that means each center must have the same variational freedom in describing the electrons formally attributed to the center. Basis sets of different quality on different atoms (minimal basis sets on some atoms and split valence + polarization on others) may give spurious effects, exploited during the SCF iterations, and driving to solution not converging.

จุฬาลงกรณ์มหาวิทยาลัย
Chulalongkorn University

2.1.4 Effective core pseudopotential (ECP)

The use of ECP has been the important success in the molecular orbital calculations involving large atoms or transition metals. ECP is simply a group of potential functions that substitute the inner shell electrons and orbitals that are normally implicit to have minor effects on the formation of chemical bonds. Investigation of the valence electrons using ECP can be carried out at a fraction of the

computational cost that is required for an all-electron calculation, whereas the overall quality of computation does not differ much from the all-electron calculations [55].

2.2 Dispersion-corrected density functional theory (D-DFT) method

The proper description of noncovalent interactions requires the inclusion of long-range electron correlation effects that are missing in both HF and DFT methods. In particular, the treatment of the weak London forces is crucial because of their attractive and ubiquitous nature. They play a critical role in many phenomena such as the crystal packing of molecular solids and the physisorption of molecules on surfaces or in microporous materials. A way to account for the missing dispersion energy in DFT is to augment the total energy as computed for a given density functional approximated method with a dispersion term [55]:

$$E^{DFT-D} = E^{DFT} + E_{Disp} \tag{2.19}$$

An efficient and cost-effective approach is to use a simple pairwise (i.e. 2-body) correction that includes the long-range dispersion energy through the asymptotic series: (i.e. $-\frac{C_6}{R^6} - \frac{C_6}{R^6} - \frac{C_6}{R^6} - \cdots$) as:

จุฬาลงกรณ์มหาวิทยาลัย
Chulalongkorn University

$$E^{Disp} = -\sum_{AB}\sum_{n=6,8,10}\left(\frac{C_n^{AB}}{R_{AB}^n}\right) \tag{2.20}$$

where C_n^{AB} are the *n*-order dispersion coefficients for a given atom pairs *AB*.

CHAPTER III
MODELS AND METHODS

3.1 Computational method

Structures of (5,5) BeONT, (10,0) BeONT, their surfaces doped by selected elements of periods 2 (B, C, and N), 3 (Mg, Al, Si, P, and S), and 4 (Ca, Ga, Ge, As and Se), and structures of their hydrogen molecule adsorption, have been optimized by periodic density functional theory (DFT) method including London-type empirical correction for dispersion interactions[56] which is called as the D2 version of Grimme's dispersion method. The empirical parameters of the D2 method of Grimme for the elements used in this work are shown in Table S1 in Appendices.

The PBE GGA functionals, Perdew-Becke-Ernzerhof (PBE) exchange, and correlation[57] , based on the expansion of the crystalline orbitals, have been employed using the CRYSTAL14 software package[58]. The 6-211d1G basis set was used for Be and O atoms. The m-6-311G(d) basis set was used for B, C, N, Mg, Al, Si, P, and S dopant atoms, m-S-RSC for Ca and m-pVDZ-PP basis set for Ga, Ge, As, and Se dopant atoms[59]. The 5-11G* basis set was used for the H atom of molecular hydrogen gas[60]. All basis sets were taken from the CRYSTAL14 homepage. The tolerances for geometry optimization convergence, truncation threshold of 10^{-8}, 10^{-8}, 10^{-8}, 10^{-9}, and 10^{-30} for the coulomb exchange were selected, and Fock/Kohn-Sham matrices mixing was set to 30. The Monkhorst-Pack shrinking factor of 10×10×1 k–point was used to sample the Brillouin zone.

The BeONTs were constructed by rolling up the 2D BeO graphene-like sheet using the hexagonal lattice parameters, a = b = 2.662 Å and α = 60º, and fractional coordinates ($\frac{1}{3}$, $\frac{1}{3}$, 0.000) for Be atom and (-$\frac{1}{3}$, -$\frac{1}{3}$, 0.000) for O atom using the SLAB and NANOTUBE keywords. The (5,5) and (10,0) BeONTs were obtained by setting the roll-up-vectors to [5 5] and [10 0] using the NANOTUBE keyword, respectively.

The (4×0×0) and (2×0×0) supercells were set for the (5,5) and (10,0) BeONTs, which consist of 80 atoms ($Be_{40}O_{40}$), respectively.

All studied structures were fully optimized at room temperature (298.15) and 1 atm using the CRYSTAL14 software package. The partial charges of atoms in molecules were obtained from the Mülliken population analysis as implemented in the CRYSTAL14 software package. Finally, all the molecular images were plotted by using the VESTA 3.4.0 software[61].

Doping of the B, Mg, Al, Ca, and Ga atoms which are designated as metal elements, on the BeONT, was modeled by replacing the Be atom with a dopant atom and doping of the N, P, S, Se, and As atoms which are selected as non-metal elements, was modeled by replacing a dopant atom to the O atom. The C, Si, and Ge can behave like the electron donor and acceptor atoms that are situated in between the electron-deficient (B, Al, and Ga) and electron-rich (N, P, and As) atoms, as shown in Figure S1, in Appendix. For doping of the C, Si, and Ge atoms, two doping structures of which a dopant atom was substituted for the Be atom and O atom were modeled.

The doping energies, ΔE_{doping} of the M dopant (M= B, C, N, Mg, Al, Si, P, S, Ca, Ga, Ge, As and Se) on the BeONT to synthesize M-BeONT is defined as shown in equation (3.1).

จุฬาลงกรณ์มหาวิทยาลัย
CHULALONGKORN UNIVERSITY

$$\Delta E_{doping} = E_{M^{(X)}\text{-BeONT}} - (E_M + E_{[BeONT+\ V_X]}) \quad (3.1)$$

where the E_M and $E_{[BeONT+\ V_X]}$ are the total energies of M atom and Be- or O-vacancy BeONT (denoted by [BeONT+ V_X]), respectively. $E_{M^{(X)}\text{-BeONT}}$ is the total energy of the $M^{(X)}$-BeONT of which $M^{(X)}$ is the M replacing to the x-vacancy of the [BeONT+ V_X].

The adsorption energy of the H_2 on the M-BeONT surface is defined as shown in equation (3.2).

$$\Delta E_{ads} = E_{H_2/\text{M-BeONT}} - (E_{H_2} + E_{[\text{M-BeONT}]}) \quad (3.2)$$

where $E_{H_2/\text{M-BeONT}}$ is the total energy of the H_2/M-BeONT. E_{H_2} and $E_{[\text{M-BeONT}]}$ are the total energies of hydrogen gas and clean M-BeONT surface, respectively

The charge-change (Δq) is defined as a charge difference between the observed atom of the M-BeONT surface after adsorbing H_2 and the clean surface, as shown in equation (3.3).

$$\Delta q = q_f - q_i \quad (3.3)$$

where q_f and q_i are charges of the observed atom of the M-BeONT surface after adsorbing H_2 and the clean M-BeONT surface, respectively.

The change of energy gap in percent (ΔE_g) is defined as a difference between H_2 adsorbed M-BeONT surface and the clean surface, as shown in equation (3.4).

$$\Delta E_g = \frac{[E_g(H_2/\text{M-BeONT}) - E_g(\text{M-BeONT})] \times 100}{E_g(\text{M-BeONT})} \quad (3.4)$$

จุฬาลงกรณ์มหาวิทยาลัย
Chulalongkorn University

where $E_g(H_2/\text{M-BeONT})$ and $E_g(\text{M-BeONT})$ are the energy gaps of the H_2/M-BeONT and M-BeONT, respectively.

The recovery time (τ), which is defined as the time taken by the sensor to achieve 90% of the total response change[62], of hydrogen adsorption sensing can be evaluated using equation (3.5)

$$\tau = \upsilon_0^{-1} e^{\left(\frac{-\Delta E_{ads}}{kT}\right)} \quad (3.5)$$

where T is the absolute temperature, k is Boltzmann's constant, and is the attempt frequency υ_0 which value of $\approx 1.0 \times 10^{12}$ s^{-1} for a gas molecule. Equation (3.5) shows that low adsorption energy (strong adsorption) of hydrogen on the material surfaces leads to a long recovery time, resulting in poor sensing material. On the other hand, the high adsorption energy of hydrogen on the material surface results in good sensing material.

จุฬาลงกรณ์มหาวิทยาลัย
Chulalongkorn University

CHAPTER IV
RESULTS AND DISCUSSIONS

4.1 Adsorption on (5,5) BeONT and its doping derivatives

4.1.1 The structures of the pristine (5,5) BeONT and periods 2–4 elements doped (5,5) BeONT surfaces

The optimized parameters of the pristine (5,5) BeONT (a = b = 2.682 Å, and α = 60^{o}) were obtained, and the optimized structure is shown in **Figure 4.1**. The diameter of the pristine (5,5) BeONT of 7.41 Å, Be-O bond lengths of 1.55 Å, O-Be-O =119.2^{o}, and Be-O-Be= 120.3^{o} were found. The optimized structures of (5,5) BeONT doped by period 2 (B, C, and N), period 3 (Mg, Al, Si, P, and S), period 4 (Ca, Ga, Ge, As, and Se) elements are shown in **Figures 4.2**, **4.3**, and **4.4**, respectively. The B–, $C^{(Be)}$–, $C^{(O)}$– and N–doped (5,5) BeONTs (**Figure 4.2**), Mg–, Al–, $Si^{(Be)}$–, $Si^{(O)}$–, P–and S–doped (5,5) BeONTs (**Figure 4.3**) and Ca–, Ga–, $Ge^{(Be)}$–, $Ge^{(O)}$–, As– and Se–doped (5,5) BeONTs (**Figure 4.4**) were found. The bond lengths of B-O (1.50, 1.50, 1.49 Å), C-O (1.54, 1.54, 1.54 Å), C-Be (1.68, 1.68, 1.79 Å), and N-Be (1.61, 1.61, 1.62 Å) of the B–, $C^{(Be)}$–, $C^{(O)}$– and N–doped (5,5) BeONTs, respectively, were found. The bond lengths of Mg-O (1.86, 1.86, 1.89 Å), Al-O (1.82, 1.82, 1.84 Å), Si-O (1.81, 1.81, 1.84 Å), Si-Be (2.16, 2.16, 2.74 Å), P-Be (2.18, 2.18, 2.13 Å) and S-Be (2.01, 2.01, 2.06 Å) of the Mg–, Al–, $Si^{(Be)}$–, $Si^{(O)}$–, P–and S–doped (5,5) BeONTs, respectively, were obtained. The bond lengths of Ca-O (2.11, 2.11, 2.15 Å), Ga-O (1.93, 1.93, 1.96 Å), Ge-O (1.96, 1.96, 1.99 Å), Ge-Be (2.40, 2.40, 2.29 Å), As-Be (2.28, 2.28, 2.24 Å) and Se-Be (2.15, 2.15, 2.21 Å) of the Ca–, Ga–, $Ge^{(Be)}$–, $Ge^{(O)}$–, As– and Se–doped (5,5) BeONTs, respectively, were obtained. Bonds of all the element-doped (5,5) BeONTs of which an atom was connected to the dopant atom are categorized into two types, two symmetrical bonds, and one unsymmetrical bond, as shown in **Figures 4.2**, **4.3** and **4.4**.

จุฬาลงกรณ์มหาวิทยาลัย
CHULALONGKORN UNIVERSITY

Plots of doping energy of period 2, period 3, and period 4 elements on the Be- or O-vacancies in the (5,5) BeONT are shown in **Figure 4.5**. The curves were categorized into the series of doping on the Be- and O-vacancy in the (5,5) BeONT, respectively. The doping energies of all the doping on the Be-vacancy are much lower than on the O-vacancy. The lowest doping energies for the dopants of period 2, period 3, and period 4 elements are respectively the B, Si, and Ca on the Be vacancy in the (5,5) BeONT, of which the values are -12.47, -12.46, and -12.99 eV (see **Table 4.1**), respectively.

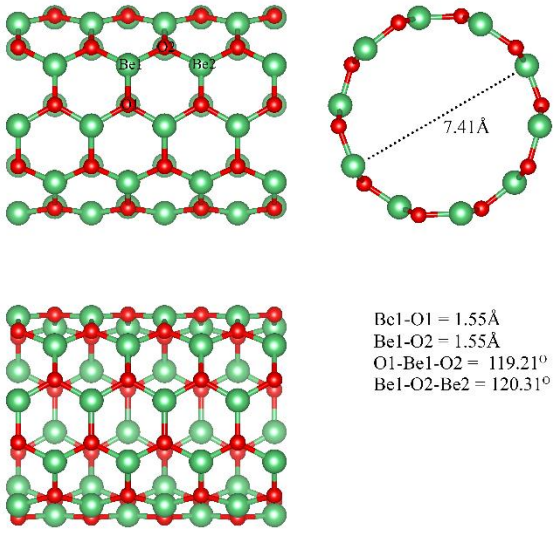

Figure 4.1 Optimized structure of the pristine (5,5) BeONT. Left and right are two different side views and front views, respectively.

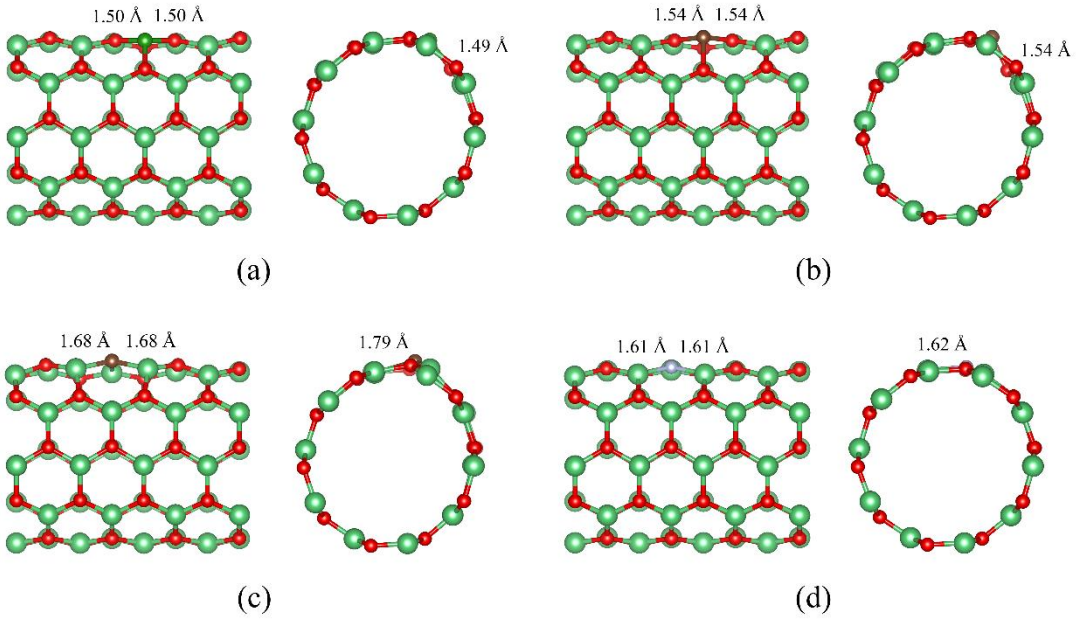

Figure 4.2 Optimized structures of the (a) B–, (b) $C^{(Be)}$ –, (c) $C^{(O)}$ – and (d) N–doped (5,5) BeONTs. Left and right images are side and front views, respectively.

จุฬาลงกรณ์มหาวิทยาลัย
Chulalongkorn University

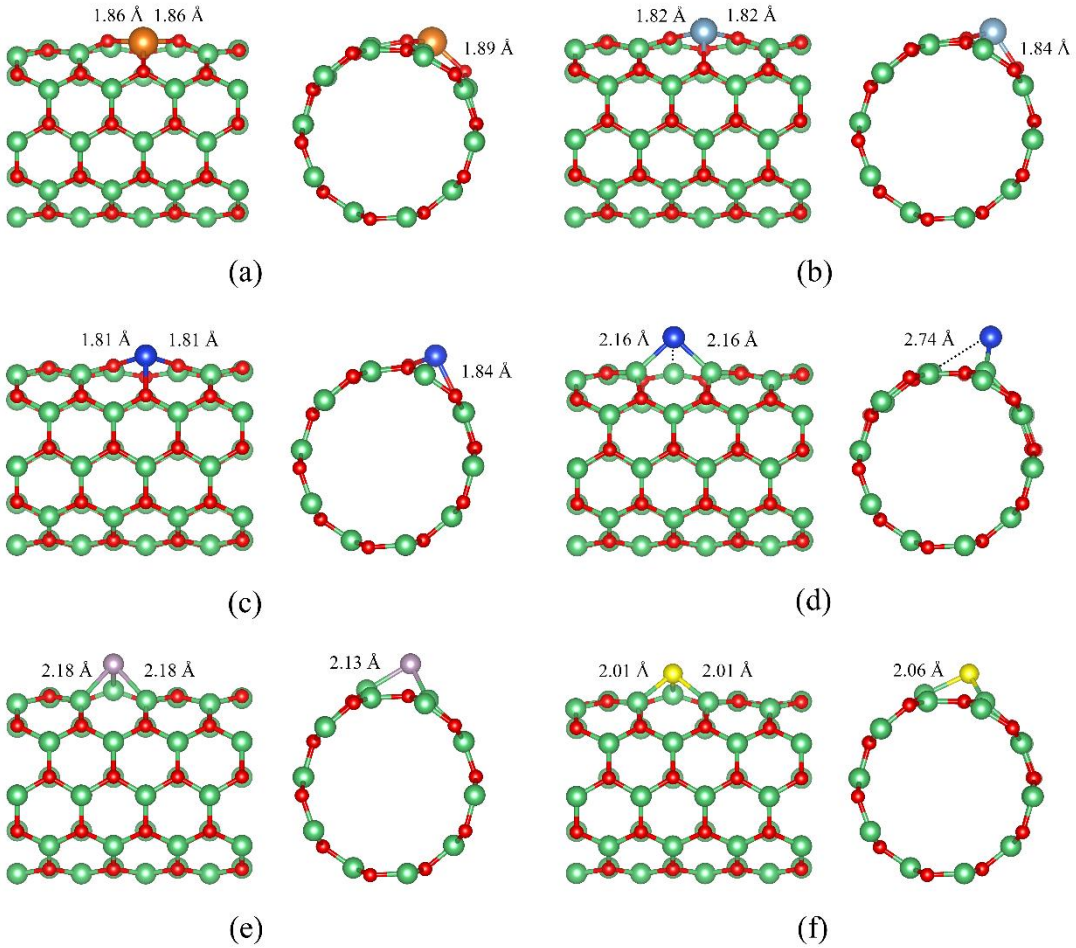

Figure 4.3 Optimized structures of the (a) Mg–, (b) Al–, (c) $Si^{(Be)}$ –, (d) $Si^{(O)}$–, (e) P– and (f) S–doped (5,5) BeONTs. Left and right images are side and front views, respectively.

จุฬาลงกรณ์มหาวิทยาลัย
Chulalongkorn University

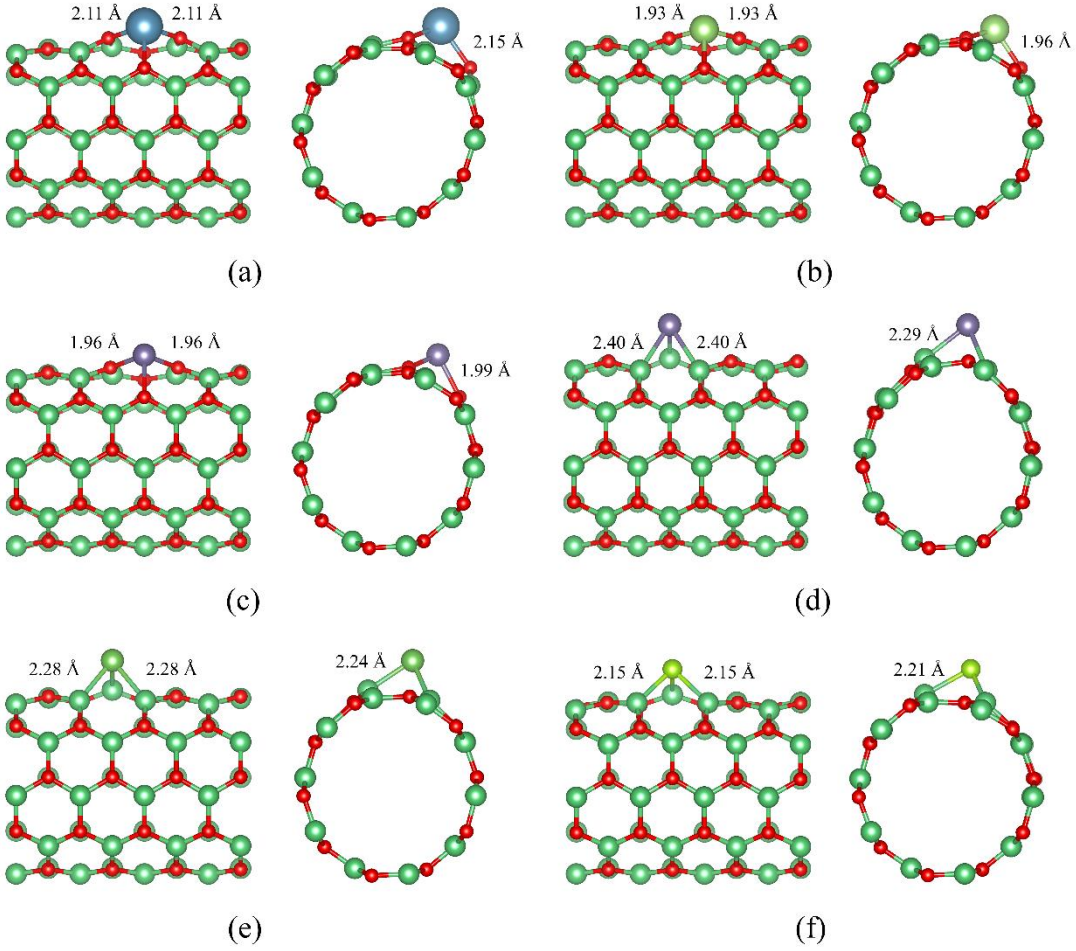

Figure 4.4 Optimized structures of the (a) Ca–, (b) Ga–, (c) $Ge^{(Be)}$ –, (d) $Ge^{(O)}$–, (e) As–and (f) Se–doped (5,5) BeONTs. Left and right images are side and front views, respectively.

จุฬาลงกรณ์มหาวิทยาลัย
Chulalongkorn University

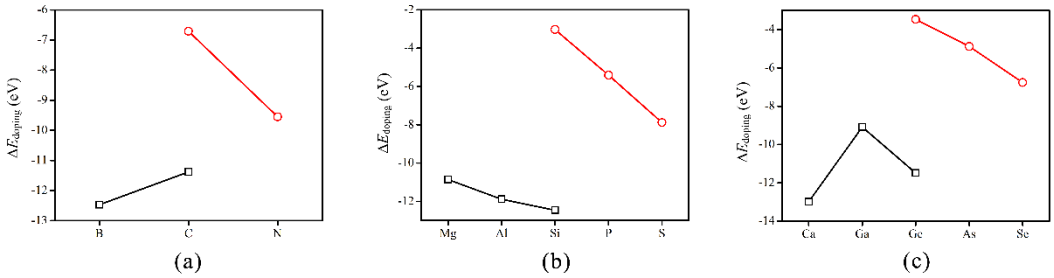

Figure 4.5 Plots of doping energy of the (5,5) BeONT doped by the (a) period 2, (b) period 3 and (c) period 4 element. Their upper and lower curves are of the doping on the O and Be vacancies in the (5,5) BeONT, respectively.

จุฬาลงกรณ์มหาวิทยาลัย
CHULALONGKORN UNIVERSITY

4.1.2 Adsorption of the hydrogen molecule on the pristine (5,5) BeONT and periods 2–4 elements–doped (5,5) BeONT surfaces

The adsorption structure of hydrogen molecule on the pristine (5,5) BeONT is shown in **Figure 4.6**. The shortest bond distances between hydrogen molecule and atoms of the pristine (5,5) BeONT are H···O = 2.70 Å and H···Be = 2.99 Å. The hydrogen adsorption on the pristine (5,5) BeONT, of which adsorption energy of –0.10 eV (see **Table 4.2**) was the physisorption.

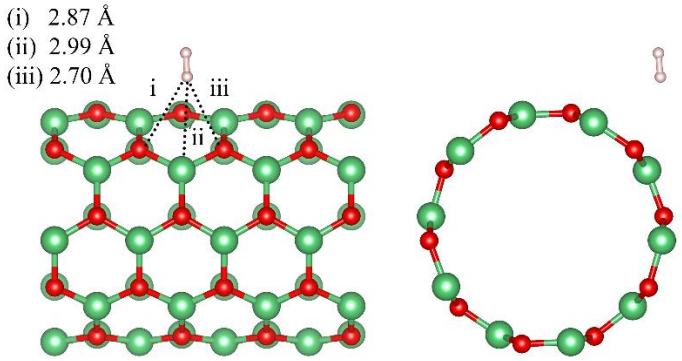

Figure 4.6 Adsorption structure of H_2 adsorbed on the pristine (5,5) BeONT. Left and right are two different side views and front views, respectively.

จุฬาลงกรณ์มหาวิทยาลัย
Chulalongkorn University

4.1.2.1 Period 2 elements

The adsorption structure of hydrogen molecule on the period 2 (B, $C^{(Be)}$, $C^{(O)}$ and N), period 3 (Mg, Al, $Si^{(Be)}$, $Si^{(O)}$, P and S), and period 4 (Ca, Ga, $Ge^{(Be)}$, $Ge^{(O)}$, As and Se) element–doped (5,5) BeONTs are shown in **Figures 4.7**, **4.8**, and **4.9**, respectively. The physical adsorptions of hydrogen molecule on the B–, $C^{(Be)}$– and N– doped (5,5) BeONT, of which adsorption energies, respectively, are –0.36, –0.22, and –0.11 eV, are shown in **Figures 4.7 (a)**, **(b)** and **(d)**, respectively. The adsorption of hydrogen molecule on the $C^{(O)}$–doped (5,5) BeONT (**Figure 4.7 (c)**) of which adsorption energy is ΔE_{ads} = –4.73 eV, was the dissociative chemisorption and their H1-C and H2-C bond lengths are 2.11 and 2.15 Å, respectively. The dissociative chemisorption of hydrogen molecule on the $C^{(O)}$–(5,5) BeONT was found as carbohydride structure. It was found that atomic charges of B (q_f = 0.722 e) of the B–(5,5) BeONT and C (q_f = 0.387 e) of the $C^{(Be)}$–(5,5) BeONT are more positive after adsorbing hydrogen molecule, but of N (q_f = -0.960 e) of the N–(5,5) BeONT and C (q_f =-0.696 e) of the $C^{(O)}$–(5,5) BeONT are more negative after hydrogen adsorption, as shown in **Table 4.3**. The largest charge-change (Δq = -0.401 e) of C adsorption center of the $C^{(O)}$–(5,5) BeONT of which hydrogen adsorption (ΔE_{ads}= –4.73 eV) is the strongest, was found; the large charge-change (Δq =+0.198 e, of which H1=+0.103 e and H2=0.095 e) of hydrogen molecule also confirmed its dissociative chemisorption.

จุฬาลงกรณ์มหาวิทยาลัย
Chulalongkorn University

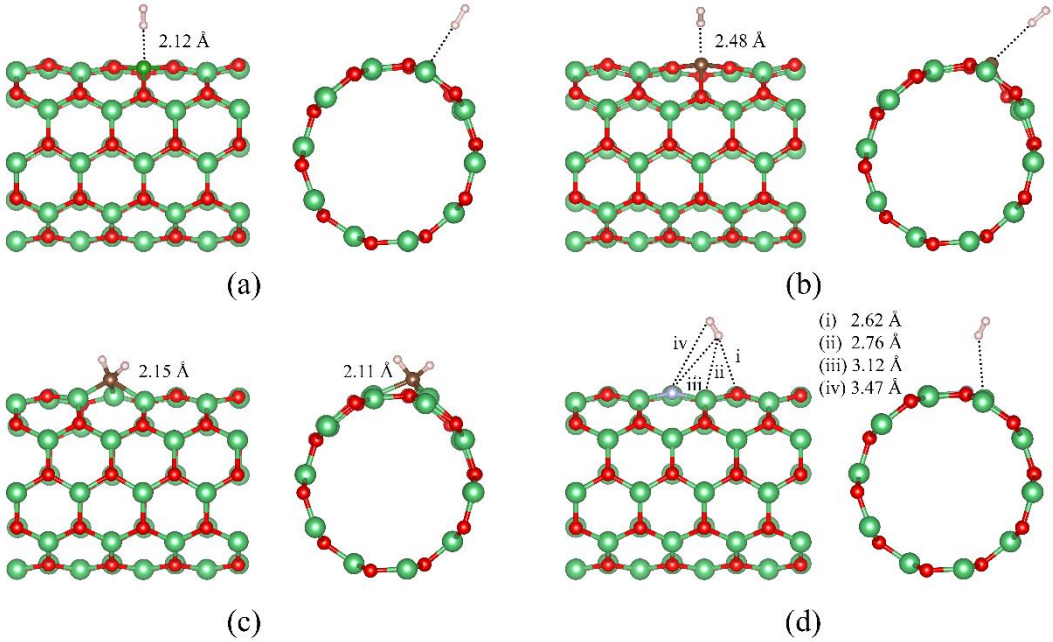

Figure 4.7 Adsorption structures of H_2 adsorbed on the (a) B–, (b) $C^{(Be)}$ –, (c) $C^{(O)}$ – and (d) N–doped (5,5) BeONTs. Left and right images are side and front views, respectively.

จุฬาลงกรณ์มหาวิทยาลัย
Chulalongkorn University

4.1.2.2 Period 3 elements

Doping with period 3 elements, adsorptions of hydrogen molecule on the Mg–, Al–, $Si^{(Be)}$–, P– and S–doped (5,5) BeONTs are physisorption of which adsorption energies, respectively, are –0.22, –0.35, –0.10, –0.12 and –0.10 eV, but on the $Si^{(O)}$–doped (5,5) BeONT is dissociative chemisorption (ΔE_{ads} = –2.92 eV) to form the silicon hydride structure.

Hydrogen-bond distances between hydrogen molecular atom and dopant atom of M–doped (5,5) BeONTs are in order: H···Mg (2.31 Å) < H···Al (2.62 Å) < H···P (2.99 Å) < H···$Si^{(Be)}$ (3.03 Å) < H···S (3.11 Å) (see **Figure 4.8**). The adsorption structure of H_2/$Si^{(O)}$–doped (5,5) BeONT, of which two H-Si bonds are 1.55 and 1.57 Å, is shown in **Figure 4.8 (d)**.

All the M-doped (5,5) BeONTs (Mg–, Al–, Si(Be)–, Si(O)– P– and S–doped (5,5) BeONTs) were found with positive charge-change after adsorbing hydrogen molecule. The magnitudes of charge-change of M adsorption center of all M-doped (5,5) BeONTs are in order: $Si^{(O)}$ (q_f = 0.225 e) > Al (q_f = 0.127 e) > Mg (q_f = 0.022 e) > S (q_f = 0.020 e) ~ $Si^{(Be)}$ (q_f = 0.020 e) > P (q_f = 0.006 e). It was found that the largest charge-change of $Si^{(O)}$ adsorption center of the $Si^{(O)}$–(5,5) BeONT of which hydrogen adsorption (ΔE_{ads}= –2.92 eV) is the strongest, agrees with the large charge-change (Δq = -0.397 e, of which H1=-0.196 e and H2=-0.201 e) of hydrogen molecule of which bond is dissociated and adsorbed on the Si atom.

จุฬาลงกรณ์มหาวิทยาลัย
Chulalongkorn University

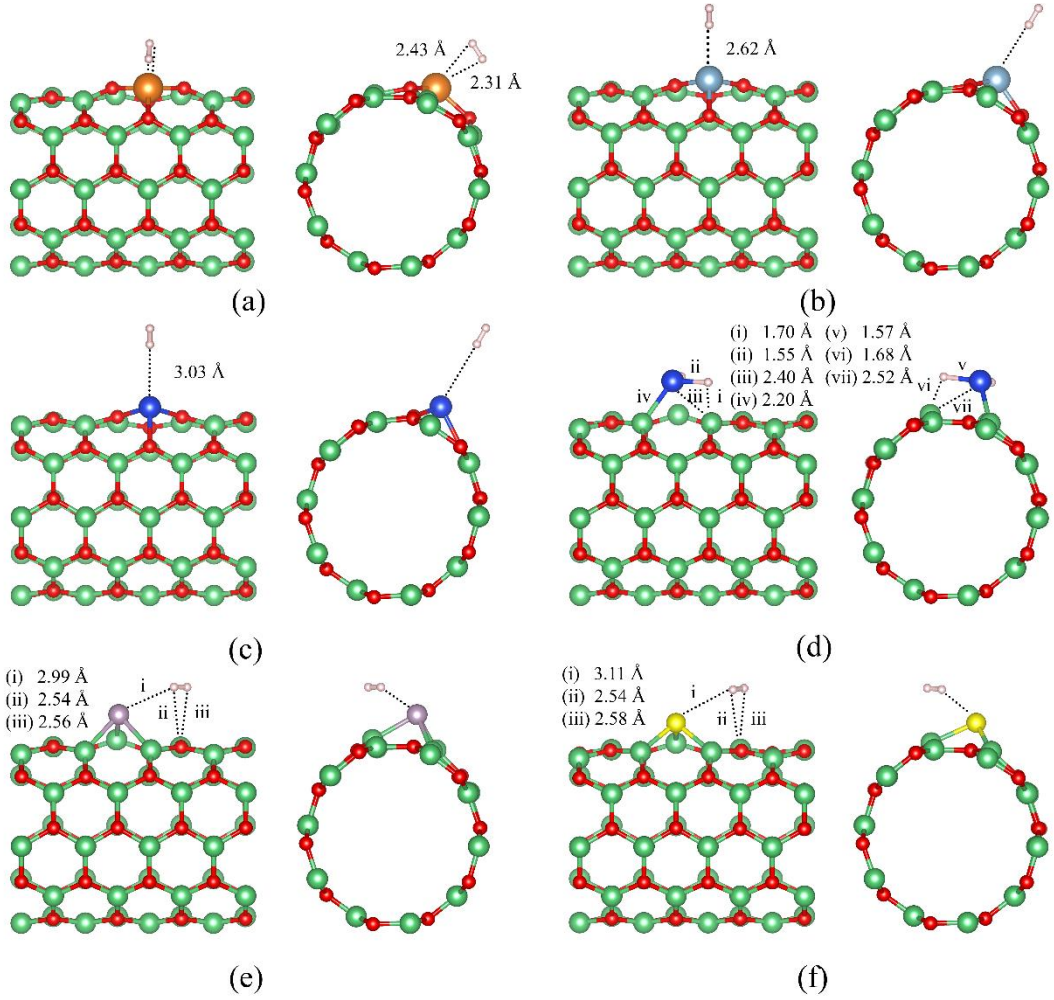

Figure 4.8 Adsorption structures of H_2 adsorbed on the (a) Mg–, (b) Al–, (c) $Si^{(Be)}$ –, (d) $Si^{(O)}$ –, (e) P– and (f) S–doped (5,5) BeONTs. Left and right images are side and front views, respectively.

Chulalongkorn University

4.1.2.3 Period 4 elements

Doping with period 4 elements, adsorptions of hydrogen molecule on the Ca–, Ga–, $Ge^{(Be)}$ –, As– and Se–doped (5,5) BeONTs are physisorption of which adsorption energies, respectively, are –0.13, –0.13, –0.08, -0.15 and –0.10 eV, but on the $Ge^{(O)}$ –doped (5,5) BeONT is dissociative chemisorption (ΔE_{ads}= –1.96 eV). Hydrogen-bond distances between the molecular hydrogen atom and dopant atom of M–doped (5,5) BeONTs are in order: H···Ca (2.69 Å) < H···Ga (2.78 Å) < H···$Ge^{(Be)}$ (3.03 Å) ~ H···As (3.03 Å) < H···Se (3.19 Å) (see **Figure 4.9**). The adsorption structure of H_2 on the $Ge^{(O)}$–doped (5,5) BeONT shows that each hydrogen atom forms two single-bonds with Si and Be atoms (-Ge-H-Be-) as the hydrogen-bridged bonds, of which two pairs of bond lengths are (Ge1-H=1.64 Å, H-Be1=1.65 Å) and (Ge2-H=1.63 Å, H-B2=1.66 Å), shown in **Figure 4.9 (d)**. Since atomic charges of adsorption site atoms including Ge atom and H_2 adsorbate of the H_2 on $Ge^{(O)}$–(5,5) BeONT which the hydrogen-bridged structure is formed, the negative atomic charges of two bridging hydrogen atoms (qH1=-0.158 e, qH2=-0.128 e) were found, as shown in **Figure S2**, in Appendix.

The charge-changes of the Ca– and Se–doped (5,5) BeONT are negative values but of the Ga–, $Ge^{(Be)}$ –, $Ge^{(O)}$ –, As–doped (5,5) BeONTs are positive value of which magnitudes are in order: $Ge^{(O)}$ (q_f = 0.110 e) > Ga (q_f = 0.053 e) > $Ge^{(Be)}$ (q_f = 0.032 e) > As (q_f = 0.000 e). It showed that the charge-change of $Ge^{(O)}$ adsorption center of the $Ge^{(O)}$ –(5,5) BeONT of which hydrogen adsorption (ΔE_{ads}= –1.96 eV) is the strongest interaction, was the largest quantity which agree with the largest charge-change (Δq = -0.306 e, of which H1=-0.158 e and H2=-0.148 e) of hydrogen molecule of which bond is dissociated and adsorbed on the Ge atom.

Plots of adsorption energy of hydrogen molecule on the (5,5) BeONT doped by periods 2, 3, and 4 elements are shown in **Figure 4.10**. The strongest adsorption of the periods 2, 3 and 4 element-doped (5,5) BeONTs are the hydrogen adsorption on the $C^{(O)}$ (ΔE_{ads} = –4.73 eV), $Si^{(O)}$ (ΔE_{ads} = –2.92 eV) and $Ge^{(O)}$ (ΔE_{ads}= –1.96 eV), respectively.

จุฬาลงกรณ์มหาวิทยาลัย
Chulalongkorn University

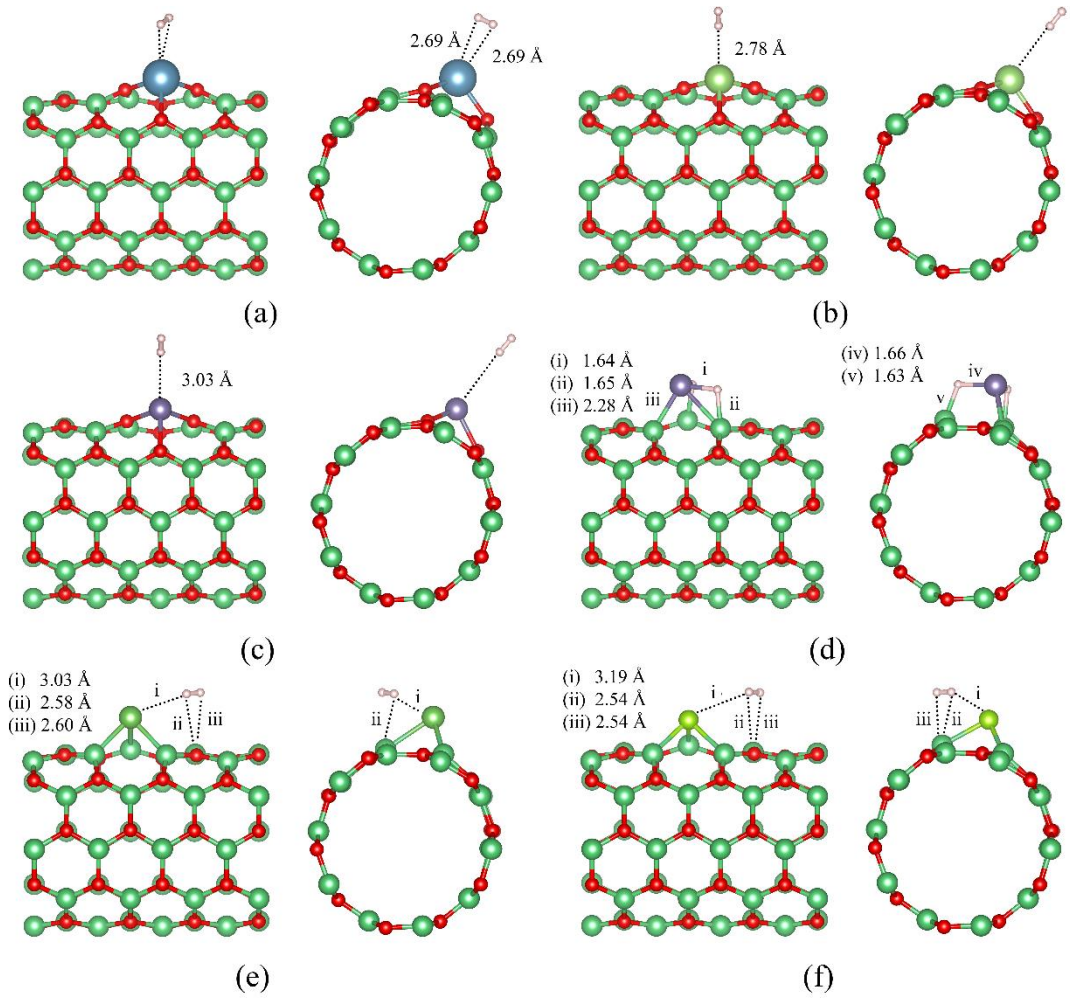

Figure 4.9 Adsorption structures of H_2 adsorbed on the (a) Ca–, (b) Ga–, (c) $Ge^{(Be)}$ –, (d) $Ge^{(O)}$ –, (e) As– and (f) Se–doped (5,5) BeONTs. Left and right images are side and front views, respectively.

จุฬาลงกรณ์มหาวิทยาลัย
Chulalongkorn University

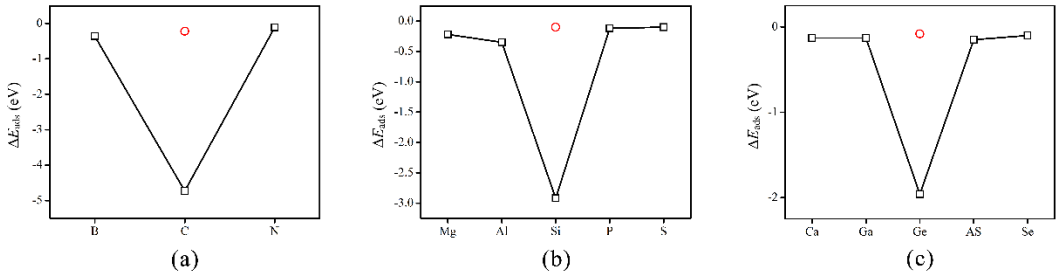

Figure 4.10 Plots of adsorption energy of hydrogen molecule on the (5,5) BeONT doped by elements of the (a) period 2, (b) period 3, and (c) period 4. The adsorptions of hydrogen molecules on the $C^{(Be)}$, $Si^{(Be)}$, and $Ge^{(Be)}$ are by the red circle.

จุฬาลงกรณ์มหาวิทยาลัย
CHULALONGKORN UNIVERSITY

4.1.3 Energy gaps of pristine and periods 2–4 elements–doped (5,5) BeONTs, and their hydrogen adsorption complexes

Energy gaps of clean surfaces of the pristine and periods 2–4 elements–doped (5,5) BeONTs, their H_2 adsorption structures, energy–gap changes after adsorption, and doping energies of the periods 2–4 elements–doped (5,5) BeONTs are shown in **Table 4.1.**

Table 4.1 shows that the energy–gap changes of adsorption structures of hydrogen molecules on the $C^{(O)}$–doped (5,5) and $Ge^{(O)}$–doped (5,5) BeONTs are dominantly high as 575.89% and 293.31%, respectively. As the adsorption of hydrogen molecule on the $C^{(O)}$–doped (5,5) and $Ge^{(O)}$–doped (5,5) BeONTs is the dissociative chemisorption, $C^{(O)}$–doped (5,5) and $Ge^{(O)}$–doped (5,5) BeONTs can, thus, be used as the hydrogen gas sensor with the short recovery time because of their high adsorption abilities, see equation (3.5). All the adsorption energies, adsorption types, and corresponding bond distances of M dopant and molecular hydrogen atom (M···H) on the M–(5,5) BeONTs, are simultaneously shown in **Table 4.2**.

จุฬาลงกรณ์มหาวิทยาลัย
Chulalongkorn University

Table 4.1 Energy gaps (E_g) and energy–gap changes of H_2 adsorption on the pristine and M–doped (5,5) BeONTs and their doping energies

Material	E_g, eV		ΔE_g, %	ΔE_{doping}, eV
	Clean surface	H_2 adsorption		
BeONT	7.11 7.75[a]	7.011	–1.39	–
Period 2:				
B–BeONT	–[b]	–[b]	–	-12.47
$C^{(Be)}$–BeONT	3.824	3.851	0.71	-11.38
$C^{(O)}$–BeONT	0.871	5.885	575.89	-6.71
N–BeONT	–[b]	–[b]	–	-9.55
Period 3:				
Mg–BeONT	6.259	6.524	4.23	-10.86
Al–BeONT	–[b]	–[b]	–	-11.89
$Si^{(Be)}$–BeONT	4.625	4.624	–0.03	-12.46
$Si^{(O)}$–BeONT	0.858	0.861	0.33	-3.03
P–BeONT	–[b]	–[b]	–	-5.41
S–BeONT	6.684	6.701	0.25	-7.88
Period 4:				
Ca–BeONT	5.725	5.147	–10.10	-12.99
Ga–BeONT	–[b]	–[b]	–	-9.09
$Ge^{(Be)}$–BeONT	5.462	5.471	0.16	-11.49
$Ge^{(O)}$–BeONT	0.939	3.693	293.31	-3.47
As–BeONT	–[b]	–[b]	–	-4.88
Se–BeONT	6.796	6.082	–10.49	-6.76

[a] Taken from ref.[28].

[b] Detected as the conductive state.

จุฬาลงกรณ์มหาวิทยาลัย
CHULALONGKORN UNIVERSITY

Table 4.2 Adsorption energies (ΔE_{ads}) of H_2 adsorption on the pristine and M–doped (5,5) BeONTs

	ΔE_{ads}, eV	Adsorption type	M–H bond length or M···H bond distance, Å
H_2/BeONT	–0.10	Physisorption	2.70 [c]
	–0.11[a]		
	–0.12[b]		
Period 2:			
H_2/B–BeONT	–0.36	Physisorption	2.12 [c]
H_2/C$^{(Be)}$–BeONT	–0.22	Physisorption	2.48 [c]
H_2/C$^{(O)}$–BeONT	–4.73	Chemisorption [d]	2.11, 2.15 [c]
H_2/N–BeONT	–0.11	Physisorption	3.12 [c]
Period 3:			
H_2/Mg–BeONT	–0.22	Physisorption	2.31 [c]
H_2/Al–BeONT	–0.35	Physisorption	2.62 [c]
H_2/Si$^{(Be)}$–BeONT	–0.10	Physisorption	3.03 [c]
H_2/Si$^{(O)}$–BeONT	–2.92	Chemisorption [e]	1.55, 1.57 [c]
H_2/P–BeONT	–0.12	Physisorption	2.99 [c]
H_2/S–BeONT	–0.10	Physisorption	3.11 [c]
Period 4:			
H_2/Ca–BeONT	–0.13	Physisorption	2.69 [c]
H_2/Ga–BeONT	–0.13	Physisorption	2.78 [c]
H_2/Ge$^{(Be)}$–BeONT	–0.08	Physisorption	3.03 [c]
H_2/Ge$^{(O)}$–BeONT	–1.96	Chemisorption [f]	1.64, 1.66 [c]
H_2/As–BeONT	– 0.15	Physisorption	3.03 [c]
H_2/Se–BeONT	–0.10	Physisorption	3.19 [c]

[a] The beryllium oxide nano–cage (BeONC) as ($Be_{12}O_{12}$), taken from ref.[63].

[b] The beryllium oxide clusters (BeOCs), namely $(BeO)_n$ (n = 2–8), taken from ref.[64].

[c] The shortest bond distance.

[d] Shown in Figure 7(c).

[e] Shown in Figure 8(d).

[f] Shown in Figure 9(d) which is the dissociative chemisorption and formed as hydrogen–bridged structure.

จุฬาลงกรณ์มหาวิทยาลัย
Chulalongkorn University

Table 4.3 Mülliken–charges (in e) of selected atoms on the M–doped (5,5) BeONTs, their H_2 adsorption complexes and changes of their charges (Δq).

Surfaces	Selected atom [a]	Clean M–BeONT q_i	H_2/M–BeONT q_f	Δq [b]
Period 2:				
B–BeONT	B	0.548	0.722	0.174
	O1	-0.702	-0.716	-0.014
	O2	-0.697	-0.714	-0.017
	O3	-0.697	-0.714	-0.017
	H1	0.000	-0.060	-0.060
	H2	0.000	-0.155	-0.155
$C^{(Be)}$–BeONT	C	0.336	0.387	0.051
	O1	-0.662	-0.663	-0.001
	O2	-0.661	-0.661	0.000
	O3	-0.661	-0.661	0.000
	H1	0.000	-0.013	-0.013
	H2	0.000	-0.084	-0.084
$C^{(O)}$–BeONT	C	-0.295	-0.696	-0.401
	Be1	0.569	0.665	0.096
	Be2	0.602	0.691	0.089
	Be3	0.569	0.656	0.087
	H1	0.000	0.103	0.103
	H2	0.000	0.095	0.095
N–BeONT	N	-0.949	-0.960	-0.011
	Be1	0.805	0.814	0.009
	Be2	0.810	0.814	0.004
	Be3	0.805	0.835	0.030
	H1	0.000	-0.029	-0.029
	H2	0.000	0.011	0.011
Period 3:				
Mg–BeONT	Mg	1.202	1.224	0.022
	O1	-0.850	-0.858	-0.008
	O2	-0.853	-0.853	0.000
	O3	-0.853	-0.853	0.000
	H1	0.000	-0.010	-0.010
	H2	0.000	-0.002	-0.002
Al–BeONT	Al	1.099	1.226	0.127
	O1	-0.863	-0.866	-0.003
	O2	-0.858	-0.863	-0.005
	O3	-0.858	-0.863	-0.005
	H1	0.000	-0.105	-0.105
	H2	0.000	-0.073	-0.073
$Si^{(Be)}$–BeONT	Si	0.783	0.803	0.020
	O1	-0.801	-0.799	0.002
	O2	-0.792	-0.790	0.002
	O3	-0.792	-0.790	0.002
	H1	0.000	-0.006	-0.006
	H2	0.000	-0.044	-0.044
$Si^{(O)}$–BeONT	Si	0.010	0.235	0.225
	Be1	0.391	0.428	0.037
	Be2	0.549	0.561	0.012
	Be3	0.390	0.524	0.134
	H1	0.000	-0.196	-0.196
	H2	0.000	-0.201	-0.201
P–BeONT	P	-0.426	-0.420	0.006
	Be1	0.575	0.548	-0.027
	Be2	0.835	0.585	-0.250
	Be3	0.575	0.593	0.018
	H1	0.000	-0.002	-0.002
	H2	0.000	-0.013	-0.013
S–BeONT	S	-0.532	-0.512	0.020
	Be1	0.634	0.618	-0.016
	Be2	0.641	0.644	0.003
	Be3	0.634	0.632	-0.002
	H1	0.000	-0.009	-0.009
	H2	0.000	-0.001	-0.001
Period 4:				
Ca–BeONT	Ca	1.142	1.127	-0.015
	O1	-0.800	-0.800	0.000

จุฬาลงกรณ์มหาวิทยาลัย
CHULALONGKORN UNIVERSITY

	O2	-0.801	-0.799	0.002
	O3	-0.801	-0.800	0.001
	H1	0.000	0.011	0.011
	H2	0.000	0.011	0.011
Ga–BeONT	Ga	0.669	0.722	0.053
	O1	-0.719	-0.721	-0.002
	O2	-0.726	-0.729	-0.003
	O3	-0.726	-0.729	-0.003
	H1	0.000	-0.037	-0.037
	H2	0.000	-0.027	-0.027
$Ge^{(Be)}$–BeONT	Ge	0.680	0.712	0.032
	O1	-0.733	-0.735	-0.002
	O2	-0.728	-0.730	-0.002
	O3	-0.728	-0.730	-0.002
	H1	0.000	-0.023	-0.023
	H2	0.000	-0.018	-0.018
$Ge^{(O)}$–BeONT	Ge	-1.054	1.056	0.110
	Be1	0.480	0.479	-0.001
	Be2	0.486	0.582	0.096
	Be3	0.480	0.574	0.094
	H1	0.000	-0.158	-0.158
	H2	0.000	-0.148	-0.148
As–BeONT	As	-0.322	-0.322	0.000
	Be1	0.563	0.606	0.043
	Be2	0.528	0.500	-0.028
	Be3	0.549	0.527	-0.022
	H1	0.000	-0.010	-0.010
	H2	0.000	-0.007	-0.007
Se–BeONT	Se	-0.458	-0.462	-0.004
	Be1	0.605	0.606	0.001
	Be2	0.614	0.618	0.004
	Be3	0.605	0.607	0.002
	H1	0.000	0.001	0.001
	H2	0.000	-0.006	-0.006

[a] Atomic labels are shown in **Figure 4.1**; four atoms in rows (1–4) and two atoms in the last two rows possess the surface and hydrogen molecules, respectively.

[b] Change of Mülliken–charges of selected atom in specific surfaces, in e, compared with a clean surface.

จุฬาลงกรณ์มหาวิทยาลัย
CHULALONGKORN UNIVERSITY

4.2 Adsorption on (10,0) BeONT and its doping derivatives

4.2.1 The structures of the pristine (10,0) BeONT and periods 2–4 elements–doped (10,0) BeONT surfaces

The optimized parameters of the pristine (10,0) BeONT (a = b = 2.608 Å, and α = 60º) were obtained and the optimized structure is shown in **Figure 4.11**. The diameter of the pristine (10,0) BeONT of 8.54 Å, Be-O bond lengths of 1.55 Å, O-Be-O = 119.38º, and Be-O-Be= 119.21º were found. The optimized structures of (10,0) BeONT doped by period 2 (B, C, and N), period 3 (Mg, Al, Si, P, and S), period 4 (Ca, Ga, Ge, As, and Se) elements are shown in **Figures 4.12**, **4.13**, and **4.14**, respectively. The B–, $C^{(Be)}$–, $C^{(O)}$– and N–doped (10,0) BeONTs (**Figure 4.12**), Mg–, Al–, $Si^{(Be)}$–, $Si^{(O)}$–, P–and S–doped (10,0) BeONTs (**Figure 4.13**) and Ca–, Ga–, $Ge^{(Be)}$–, $Ge^{(O)}$–, As– and Se–doped (10,0) BeONTs (**Figure 4.14**) were found. The bond lengths of B-O (1.50, 1.50, 1.50 Å), C-O (1.55, 1.55, 1.55 Å), C-Be (1.73, 1.73, 1.72 Å), and N-Be (1.61, 1.61, 1.61 Å) of the B–, $C^{(Be)}$–, $C^{(O)}$– and N–doped (10,0) BeONTs, respectively, were found. The bond lengths of Mg-O (1.86, 1.88, 1.88 Å), Al-O (1.81, 1.83, 1.83 Å), Si-O (1.81, 1.83, 1.83 Å), Si-Be (2.19, 2.64, 2.12 Å), P-Be (2.09, 2.11, 2.15 Å) and S-Be (2.09, 2.19, 2.19 Å) of the Mg–, Al–, $Si^{(Be)}$–, $Si^{(O)}$–, P– and S–doped (10,0) BeONTs, respectively, were obtained. The bond lengths of Ca-O (2.11, 2.13, 2.13 Å), Ga-O (1.92, 1.95, 1.95 Å), Ge-O (1.95, 1.98, 1.98 Å), Ge-Be (2.38, 2.47, 2.47 Å), As-Be (2.21, 2.22, 2.37 Å) and Se-Be (2.13, 2.19, 2.19 Å) of the Ca–, Ga–, $Ge^{(Be)}$–, $Ge^{(O)}$–, As– and Se–doped (10,0) BeONTs, respectively, were obtained. Bonds of all the element-doped (10,0) BeONTs of which an atom was connected to the dopant atom are categorized into two types, two symmetrical bonds, and one unsymmetrical bond, as shown in **Figures 4.12**, **4.13**, and **4.14**.

Plots of doping energy of period 2, period 3, and period 4 elements on the Be- or O-vacancies in the (10,0) BeONT are shown in **Figure 4.15**. The curves were categorized into the series of doping on the Be and O vacancy in the (10,0) BeONT, respectively. The doping energies of all the doping on the Be-vacancy are much lower than on the O-vacancy. The lowest doping energies for the dopants of period 2, period 3, and period 4 elements are respectively the B, Si, and Ca on the Be vacancy in the

จุฬาลงกรณ์มหาวิทยาลัย
Chulalongkorn University

(10,0) BeONT, of which the values are -12.49, -12.47, and -13.04 eV (see **Table 4.4**), respectively.

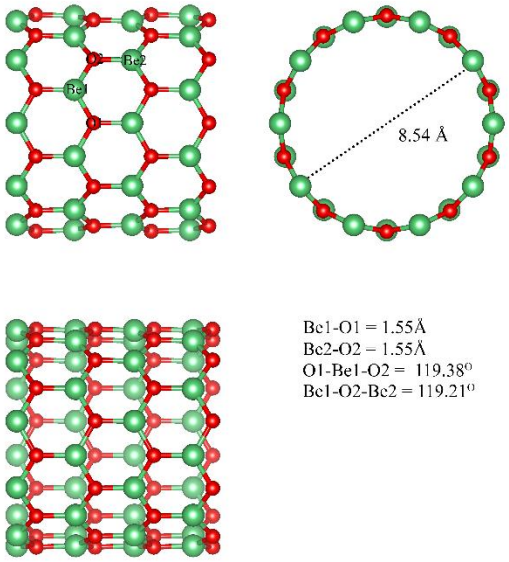

Figure 4.11 Optimized structures of the pristine (10,0) BeONTs. Left and right images are two different side and front views, respectively.

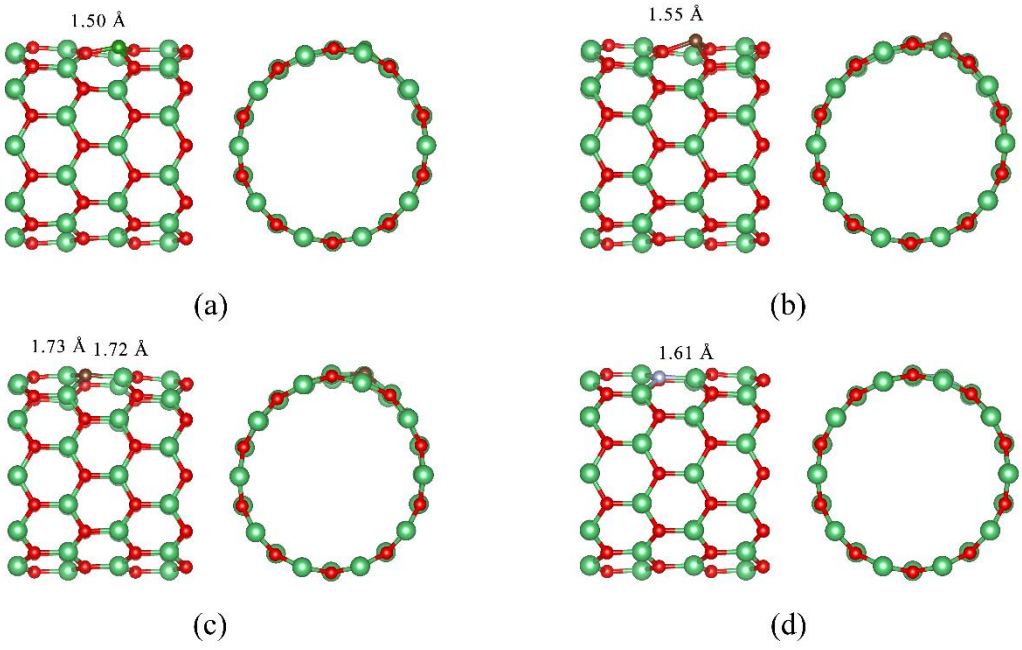

Figure 4.12 Optimized structures of the (a) B–, (b) $C^{(Be)}$–, (c) $C^{(O)}$– and (d) N–doped (10,0) BeONTs. Left and right images are side and front views, respectively.

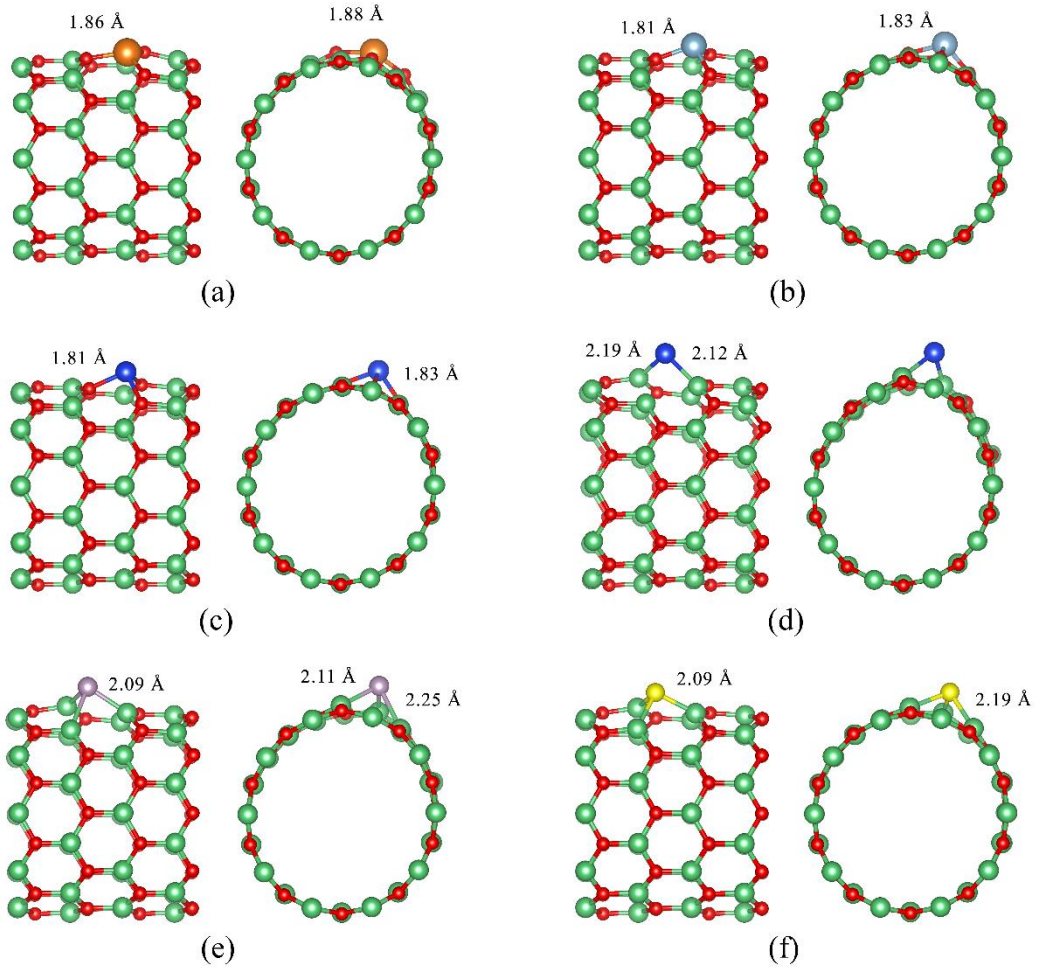

จุฬาลงกรณ์มหาวิทยาลัย
Chulalongkorn University

Figure 4.13 Optimized structures of the (a) Mg–, (b) Al–, (c) $Si^{(Be)}$–, (d) $Si^{(O)}$–, (e) P–and (f) S–doped (10,0) BeONTs. Left and right images are side and front views, respectively.

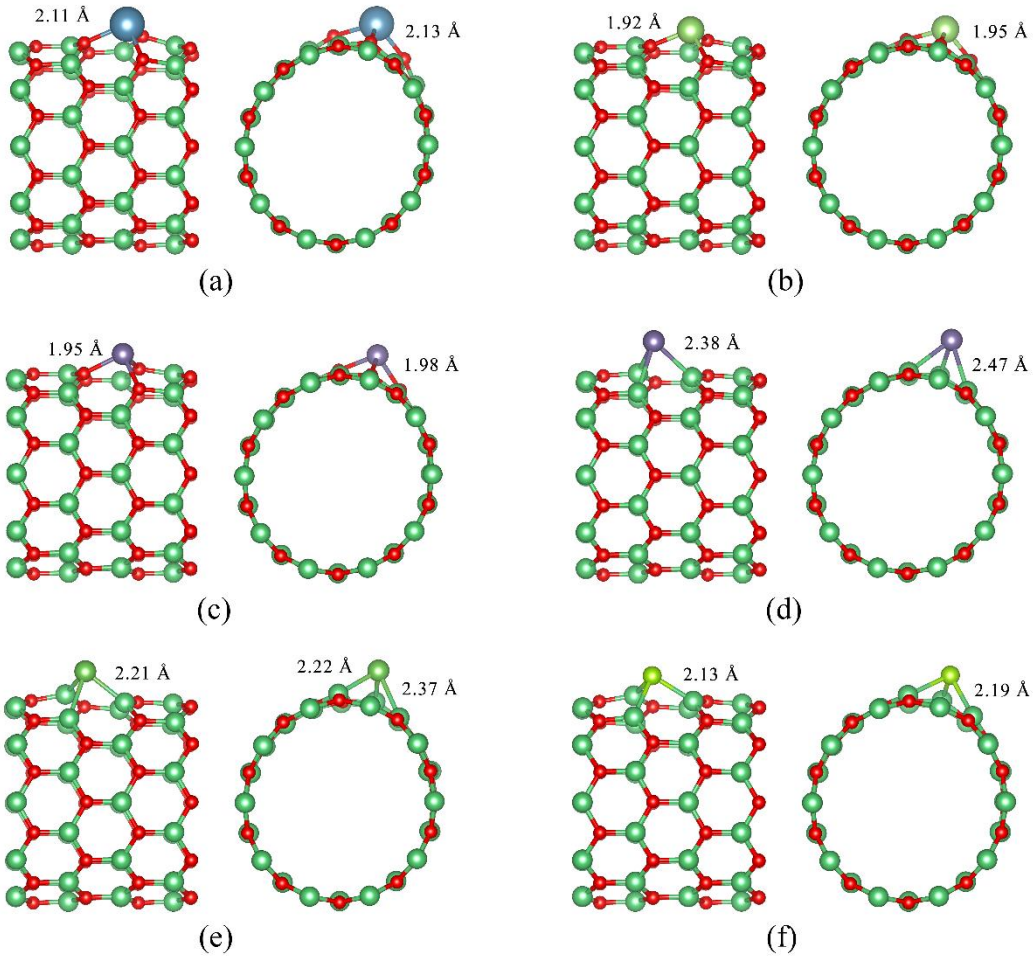

Figure 4.14 Optimized structures of the (a) Ca–, (b) Ga–, (c) $Ge^{(Be)}$–, (d) $Ge^{(O)}$–, (e) As–and (f) Se–doped (10,0) BeONTs. Left and right images are side and front views, respectively.

จุฬาลงกรณ์มหาวิทยาลัย
Chulalongkorn University

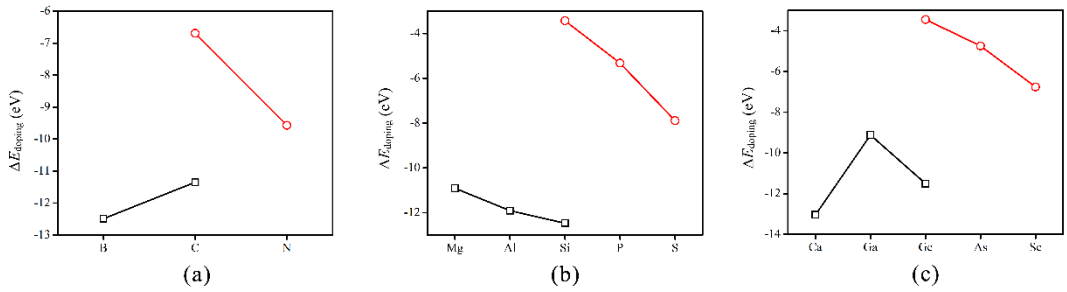

Figure 4.15 Plots of doping energy of the (10,0) BeONT doped by elements of the (a) period 2, (b) period 3, and (c) period 4. Their upper and lower curves are of the doping on the O and Be vacancies of the (10,0) BeONT, respectively.

จุฬาลงกรณ์มหาวิทยาลัย
CHULALONGKORN UNIVERSITY

4.2.2 Adsorption of the hydrogen molecule on the pristine (10,0) BeONT and periods 2–4 elements–doped (10,0) BeONT surfaces

The adsorption structure of hydrogen molecule on the pristine (10,0) BeONT is shown in **Figure 4.16**. The shortest bond distances between hydrogen molecule and adsorption site atom of the pristine (10,0) BeONT are H···O = 2.78 Å and H···Be = 2.57 Å. The hydrogen adsorption on the pristine (10,0) BeONT, of which adsorption energy of –0.08 eV (see Table 5) was the physisorption.

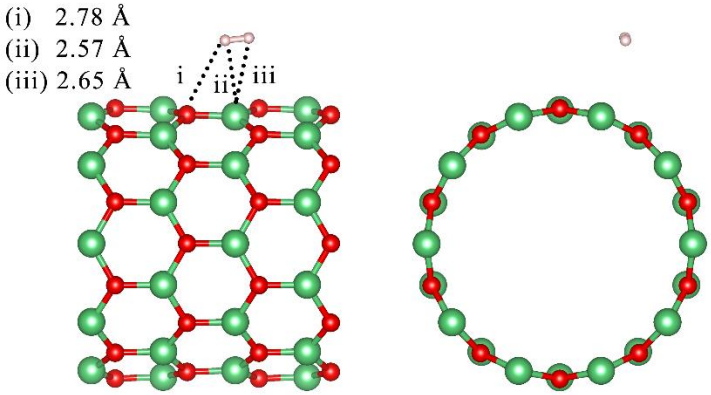

Figure 4.16 Adsorption structures of H_2 adsorbed on the pristine (10,0) BeONTs. Left and right images are side and front views, respectively.

จุฬาลงกรณ์มหาวิทยาลัย
Chulalongkorn University

4.2.2.1 Period 2 elements

The adsorption structure of hydrogen molecule on the period 2 (B, $C^{(Be)}$, $C^{(O)}$ and N), period 3 (Mg, Al, $Si^{(Be)}$, $Si^{(O)}$, P and S), and period 4 (Ca, Ga, $Ge^{(Be)}$, $Ge^{(O)}$, As and Se) element–doped (10,0) BeONTs are shown in **Figures 4.17**, **4.18**, and **4.19**, respectively. The physical adsorptions of hydrogen molecule on the B–, $C^{(Be)}$– and N–doped (10,0) BeONT, of which adsorption energies, respectively, are –0.40, –0.21, and –0.16 eV, are shown in **Figures 4.17 (a)**, **(b)** and **(d)**, respectively. The adsorption of hydrogen molecule on the $C^{(O)}$–doped (10,0) BeONT (**Figure 4.17 (c)**) of which adsorption energy is ΔE_{ads}= –4.75 eV, was the dissociative chemisorption and their H1-C and H2-C bond lengths are 2.12 Å. The dissociative chemisorption of hydrogen molecule on the $C^{(O)}$–doped (10,0) BeONT was also found as the carbohydride structure. It was found that atomic charges of B (q_f = 0.818 e) of the B–(10,0) BeONT and C (q_f = 0.387 e) of the $C^{(Be)}$–(10,0) BeONT are more positive after adsorbing hydrogen molecule, but of N (q_f = –1.091 e) of the N–(10,0) BeONT and C (q_f = –0.690 e) of the $C^{(O)}$–(10,0) BeONT are more negative after hydrogen adsorption, as shown in **Table 4.6**. Furthermore, the largest charge-change (Δq = –0.412 e) of C adsorption center of the $C^{(O)}$– (10,0) BeONT of which hydrogen adsorption is the strongest, was found; the large charge-change (Δq = +0.194 e, of which H1 = +0.097 e and H2 = +0.097 e) of hydrogen molecule also confirmed its dissociative chemisorption.

จุฬาลงกรณ์มหาวิทยาลัย
Chulalongkorn University

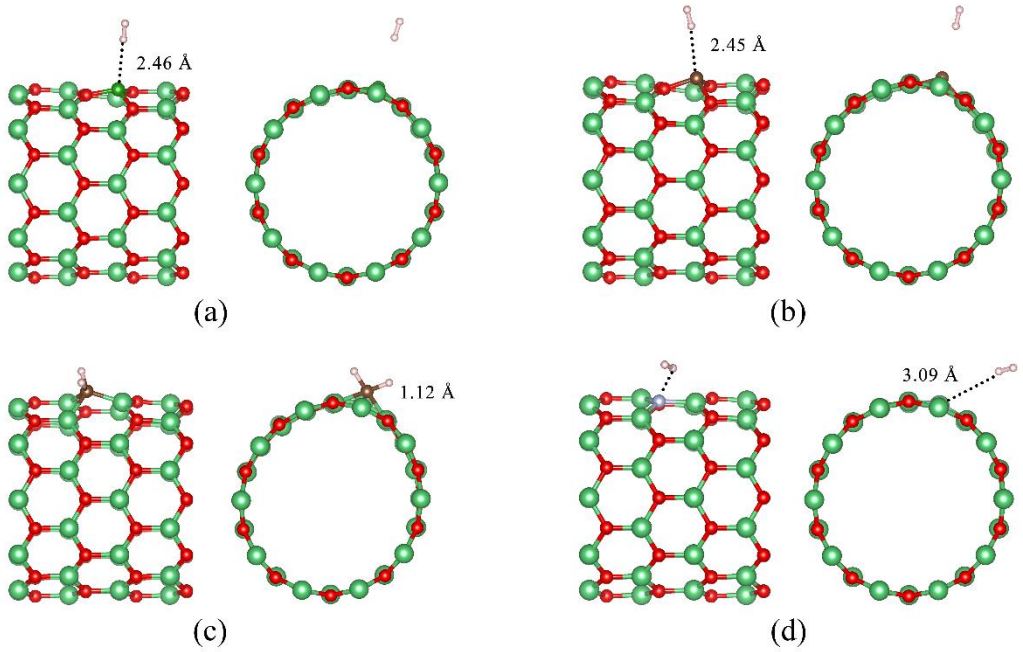

Figure 4.17 Adsorption structures of H_2 adsorbed on the (a) B–, (b) $C^{(Be)}$–, (c) $C^{(O)}$– and (d) N–doped (10,0) BeONTs. Left and right images are side and front views, respectively.

จุฬาลงกรณ์มหาวิทยาลัย
Chulalongkorn University

4.2.2.2 Period 3 elements

Doping with period 3 elements, adsorptions of hydrogen molecule on the Mg–, Al–, $Si^{(Be)}$–, P– and S–doped (10,0) BeONTs are physisorption of which adsorption energies, respectively, are –0.11, –0.36, –0.11, –0.09 and –0.11 eV, but on the $Si^{(O)}$–doped (10,0) BeONT is dissociative chemisorption (ΔE_{ads}= –2.56 eV) to form the silicon hydride structure. Hydrogen bond distances between hydrogen molecular atom and dopant atom of M–doped (10,0) BeONTs are in order: H···Mg (3.79 Å) < H···Al (2.62 Å) < H···P (2.97 Å) < H···$Si^{(Be)}$ (2.91 Å) < H···S (2.93 Å) (see **Figure 4.18**). The adsorption structure of $H_2/Si^{(O)}$–doped (10,0) BeONT, of which two H-Si bonds are 1.51 and 1.54 Å, as shown in **Figure 4.18 (d)**. All the M-doped (10,0) BeONTs (Mg–, Al–, $Si^{(Be)}$–, $Si^{(O)}$– P– and S–doped (10,0) BeONTs) were found with positive charge-change after adsorbing hydrogen molecule. The magnitudes of charge-change of M adsorption center of all M-doped (10,0) BeONTs are in order: $Si^{(O)}$ (q_f = 0.190 e) > Al (q_f = 0.129 e) > S (q_f = 0.034 e) > P (q_f = 0.029 e) > $Si^{(Be)}$ (q_f = 0.016 e) > Mg (q_f = 0.002 e). It was found that the largest charge-change of $Si^{(O)}$ adsorption center of the $Si^{(O)}$–(10,0) BeONT of which hydrogen adsorption is the strongest, agrees with the large charge-change (Δq = –0.380 e, of which H1 = –0.202 e and H2 = –0.178 e) of hydrogen molecule of which bond is dissociated and adsorbed on the Si atom.

จุฬาลงกรณ์มหาวิทยาลัย
CHULALONGKORN UNIVERSITY

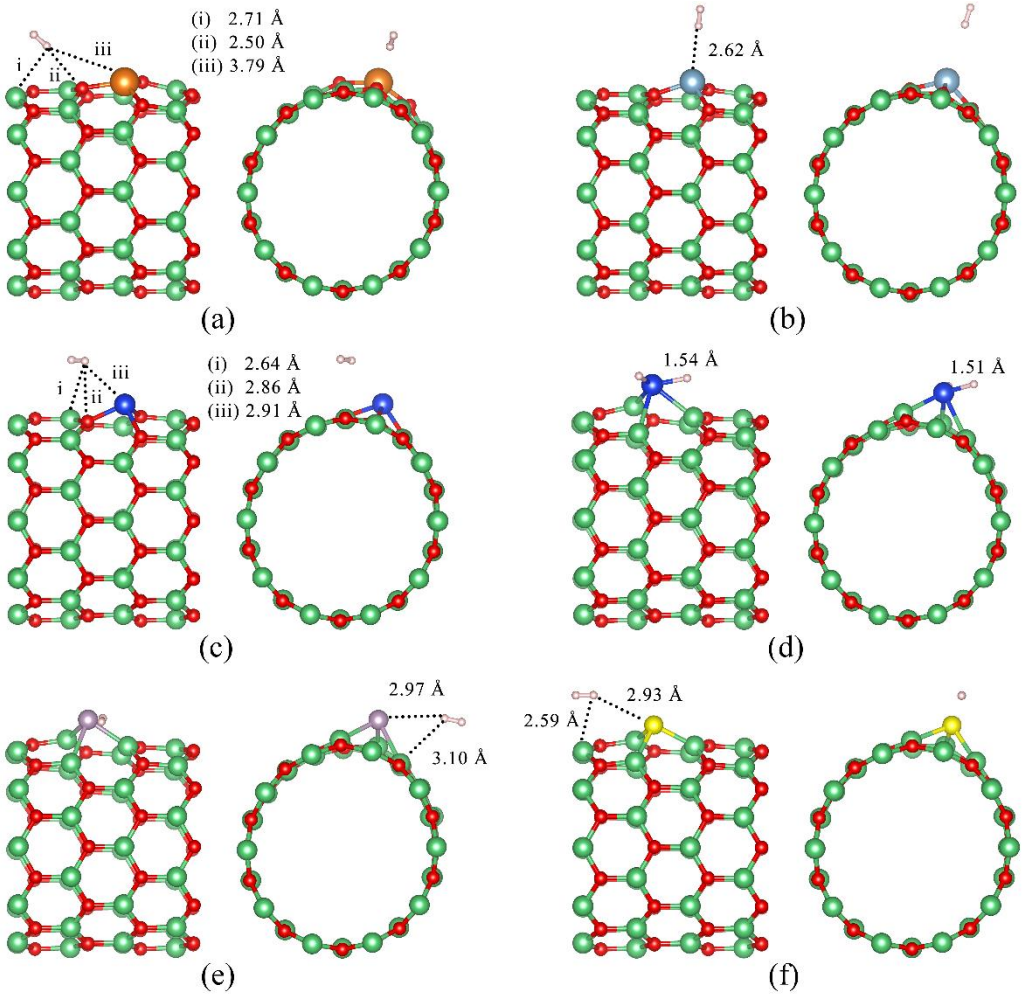

Figure 4.18 Adsorption structures of H_2 adsorbed on the (a) Mg–, (b) Al–, (c) $Si^{(Be)}$–, (d) $Si^{(O)}$–, (e) P–and (f) S–doped (10,0) BeONTs. Left and right images are side and front views, respectively.

จุฬาลงกรณ์มหาวิทยาลัย
Chulalongkorn University

4.2.2.3 Period 4 elements

Doping with period 4 elements, adsorptions of hydrogen molecule on the Ca–, Ga–, $Ge^{(Be)}$–, $Ge^{(O)}$–, As– and Se–doped (10,0) BeONTs are physisorption of which adsorption energies are –0.19, –0.13, –0.09, –0.13, –0.12 and –0.10 eV, respectively. Shortest hydrogen-bond distances between hydrogen molecular atom and dopant atom of the M–doped (10,0) BeONTs are in order: H···Ga (2.75 Å) < H···Ca (2.58 Å) < H···$Ge^{(O)}$ (2.90 Å) ~ H···As (2.90 Å) < H···Se (3.01 Å) < H···$Ge^{(Be)}$ (3.05 Å) (see **Figure 4.19**). Their adsorption abilities on hydrogen molecule are in order: Ca– (ΔE_{ads} = –0.19 eV), Ga– (ΔE_{ads} = –0.13 eV) ~ $Ge^{(O)}$– (ΔE_{ads} = –0.13 eV) > As– (ΔE_{ads} = –0.12 eV) > Se– (ΔE_{ads} = –0.10 eV) > $Ge^{(Be)}$–doped (10,0) BeONTs (ΔE_{ads} = –0.09 eV). It can be concluded that all the period 4 elements–doped (10,0) BeONTs were low adsorption ability on hydrogen molecule.

Plots of adsorption energy of hydrogen molecule on the (10,0) BeONT doped by periods 2, 3, and 4 elements are shown in **Figure 4.20**. The strongest adsorption of the period 2, period 3 and period 4 element-doped (10,0) BeONTs are the hydrogen adsorption on the $C^{(O)}$ (ΔE_{ads} = –4.75 eV), $Si^{(O)}$ (ΔE_{ads} = –2.56 eV) and Ca (ΔE_{ads} = –0.19 eV), respectively.

จุฬาลงกรณ์มหาวิทยาลัย
Chulalongkorn University

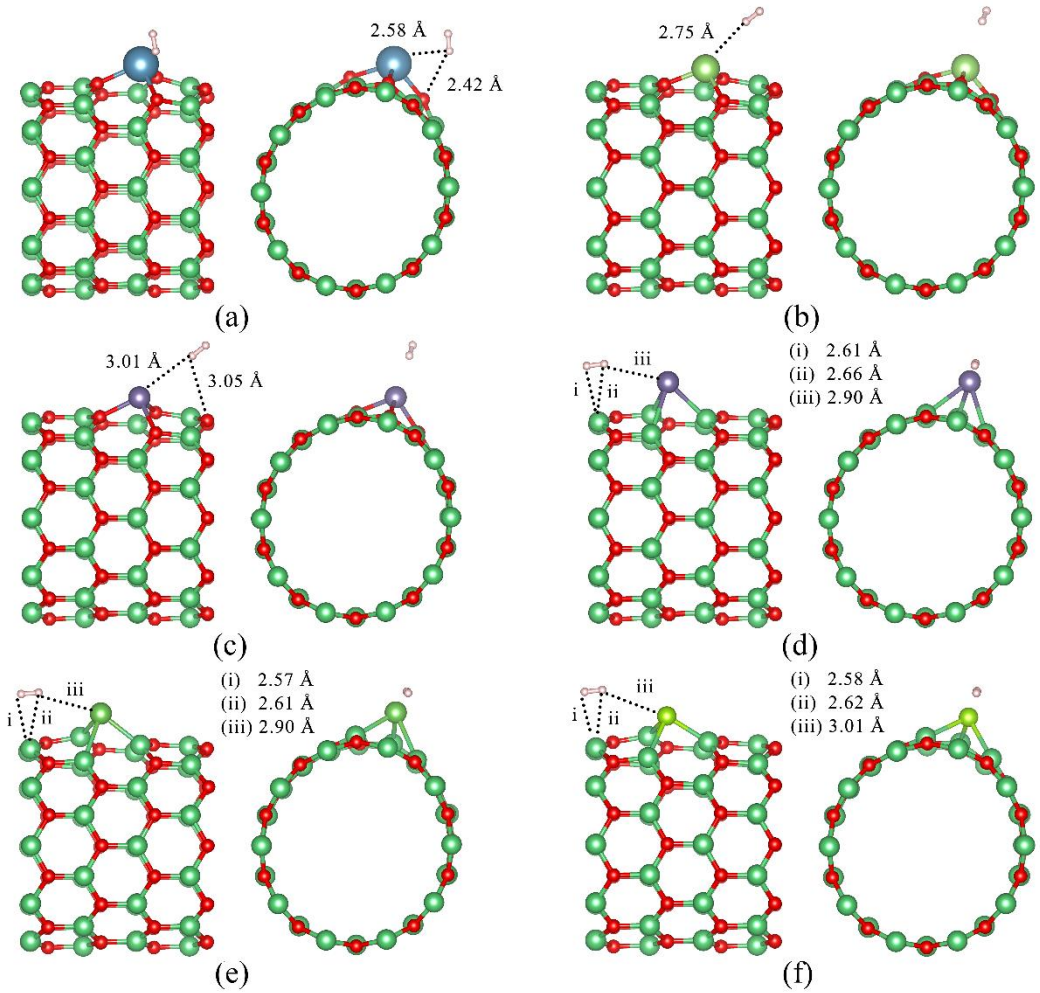

Figure 4.19 Adsorption structures of H_2 adsorbed on the (a) Ca–, (b) Ga–, (c) $Ge^{(Be)}$–, (d) $Ge^{(O)}$–, (e) As–and (f) Se–doped (10,0) BeONTs. Left and right images are side and front views, respectively.

Chulalongkorn University

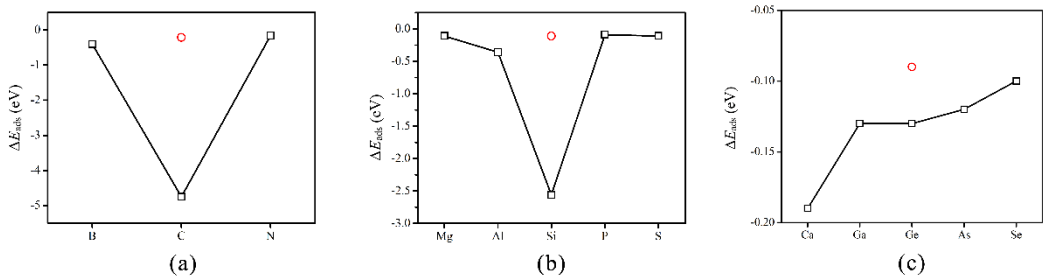

Figure 4.20 Plots of adsorption energy of hydrogen molecule on the (10,0) BeONT doped by elements of the (a) period 2, (b) period 3, and (c) period 4. The adsorptions of hydrogen molecules on the $C^{(Be)}$, $Si^{(Be)}$, and $Ge^{(Be)}$ are by the red circle.

จุฬาลงกรณ์มหาวิทยาลัย
CHULALONGKORN UNIVERSITY

4.2.3 Energy gaps of pristine and periods 2–4 elements–doped (10,0) BeONTs, and their hydrogen adsorption complexes

Energy gaps of clean surfaces of the pristine and periods 2–4 elements–doped (10,0) BeONTs, their H_2 adsorption structures, energy–gap changes after adsorption, and doping energies of the periods 2–4 elements–doped (10,0) BeONTs are shown in **Table 4.4**.

Table 4.4 shows that the largest values of energy–gap change after adsorbing hydrogen molecule on the $C^{(O)}$–, $Si^{(O)}$– and $Ge^{(O)}$–doped (10,0) BeONTs are 714.68%, 227.76%, and 94.53%, respectively. As the adsorption of hydrogen molecule on the $C^{(O)}$– and $Si^{(O)}$–doped (10,0) BeONTs is the dissociative chemisorption, the $C^{(O)}$– and $Si^{(O)}$–doped (10,0) BeONTs can, therefore, be used as the hydrogen gas sensor with short recovery time because of their high adsorption abilities. It can be suggested that the $Ge^{(O)}$–doped (10,0) BeONT could be utilized as the hydrogen gas sensor because of its intermediate adsorption ability.

All the adsorption energies, adsorption types, and corresponding bond distances of M dopant and molecular hydrogen atom (M···H) on the M-(10,0) BeONTs are simultaneously shown in **Table 4.5**.

จุฬาลงกรณ์มหาวิทยาลัย
Chulalongkorn University

Table 4.4 Energy gaps (E_g) and energy–gap changes of H_2 adsorption on the pristine and M–doped (10,0) BeONTs and their doping energies

Material	E_g, eV		ΔE_g, %	ΔE_{doping}, eV
	Clean surface	H_2 adsorption		
BeONT	7.167	7.174	0.10368	–
	8.03[a]			
	9.32[b]			
Period 2:				
B–BeONT	–[c]	–[c]	–	-12.49
$C^{(Be)}$–BeONT	3.935	3.956	0.54	-11.35
$C^{(O)}$–BeONT	0.722	5.879	714.68	-6.69
N–BeONT	–[c]	–[c]	–	-9.57
Period 3:				
Mg–BeONT	6.355	6.292	-0.98	-10.91
Al–BeONT	–[c]	–[c]	–	-11.91
$Si^{(Be)}$–BeONT	4.745	4.560	-3.90	-12.47
$Si^{(O)}$–BeONT	1.315	4.311	227.76	-3.43
P–BeONT	–[c]	–[c]	–	-5.32
S–BeONT	6.684	6.833	0.44	-7.89
Period 4:				
Ca–BeONT	5.695	5.654	-0.73	-13.04
Ga–BeONT	–[c]	–[c]	–	-9.12
$Ge^{(Be)}$–BeONT	5.579	5.377	-3.62	-11.51
$Ge^{(O)}$–BeONT	1.730	3.365	94.53	-3.45
As–BeONT	–[c]	–[c]	–	-4.75
Se–BeONT	6.189	6.198	0.16	-6.76

[a] Taken from ref.[28] .

[b] Taken from ref.[65] .

[c] Detected as the conductive state.

จุฬาลงกรณ์มหาวิทยาลัย
Chulalongkorn University

Table 4.5 Adsorption energies (ΔE_{ads}) of H_2 adsorption on the pristine and M–doped (10,0) BeONTs

Configuration	ΔE_{ads}, eV	Adsorption type	M–H bond length or M···H bond distance, Å
H_2/BeONT	–0.08	Physisorption	2.56 [c]
Period 2:			
H_2/B–BeONT	–0.40	Physisorption	2.46 [c]
H_2/$C^{(Be)}$–BeONT	–0.21	Physisorption	2.45 [c]
H_2/$C^{(O)}$–BeONT	–4.75	Chemisorption [a]	1.12, 1.12 [c]
H_2/N–BeONT	–0.16	Physisorption	3.09 [c]
Period 3:			
H_2/Mg–BeONT	–0.11	Physisorption	3.79 [c]
H_2/Al–BeONT	–0.36	Physisorption	2.62 [c]
H_2/$Si^{(Be)}$–BeONT	–0.11	Physisorption	2.91 [c]
H_2/$Si^{(O)}$–BeONT	–2.56	Chemisorption [b]	1.51, 1.54 [c]
H_2/P–BeONT	–0.09	Physisorption	2.97 [c]
H_2/S–BeONT	–0.11	Physisorption	2.93 [c]
Period 4:			
H_2/Ca–BeONT	–0.19	Physisorption	2.58 [c]
H_2/Ga–BeONT	–0.13	Physisorption	2.75 [c]
H_2/$Ge^{(Be)}$–BeONT	–0.09	Physisorption	3.01 [c]
H_2/$Ge^{(O)}$–BeONT	–0.13	Physisorption	2.90 [c]
H_2/As–BeONT	– 0.12	Physisorption	2.90 [c]
H_2/Se–BeONT	–0.10	Physisorption	3.01 [c]

[a] Shown in Figure 17(c).

[b] Shown in Figure 18(d).

[c] The shortest bond distance.

จุฬาลงกรณ์มหาวิทยาลัย
Chulalongkorn University

Table 4.6 Mülliken–charges (in e) of selected atoms on the M–doped (10,0) BeONTs, their H_2 adsorption complexes, and changes of their charges (Δq).

	Selected atom [a]	Clean M–BeONT	H_2/M–BeONT	Δq [b]
		q_i	q_f	
Period 2:				
B–BeONT	B	0.541	0.818	0.277
	O1	-0.699	-0.732	-0.033
	O2	-0.703	-0.733	-0.030
	O3	-0.703	-0.733	-0.030
	H1	0.000	-0.080	-0.080
	H2	0.000	-0.247	-0.247
$C^{(Be)}$–BeONT	C	0.339	0.387	0.048
	O1	-0.671	-0.674	-0.003
	O2	-0.667	-0.666	0.001
	O3	-0.667	-0.665	0.002
	H1	0.000	-0.008	-0.008
	H2	0.000	-0.088	-0.088
$C^{(O)}$–BeONT	C	-0.278	-0.690	-0.412
	Be1	0.582	0.673	0.091
	Be2	0.582	0.673	0.091
	Be3	0.559	0.656	0.097
	H1	0.000	0.097	0.097
	H2	0.000	0.097	0.097
N–BeONT	N	-0.956	-1.091	-0.135
	Be1	0.816	0.844	0.028
	Be2	0.816	0.844	0.028
	Be3	0.816	0.843	0.027
	H1	0.000	0.140	0.140
	H2	0.000	-0.042	-0.042
Period 3:				
Mg–BeONT	Mg	1.204	1.206	0.002
	O1	-0.855	-0.860	-0.005
	O2	-0.855	-0.856	-0.001
	O3	-0.855	-0.856	-0.001
	H1	0.000	-0.048	-0.048
	H2	0.000	0.015	0.015
Al–BeONT	Al	1.098	1.227	0.129
	O1	-0.860	-0.866	-0.006
	O2	-0.865	-0.869	-0.004
	O3	-0.865	-0.869	-0.004
	H1	0.000	-0.106	-0.106
	H2	0.000	-0.074	-0.074
$Si^{(Be)}$–BeONT	Si	0.782	0.798	0.016
	O1	-0.796	-0.804	-0.008
	O2	-0.801	-0.803	-0.002
	O3	-0.801	-0.800	0.001
	H1	0.000	-0.010	-0.010
	H2	0.000	-0.016	-0.016
$Si^{(O)}$–BeONT	Si	0.018	0.208	0.190
	Be1	0.500	0.530	0.030
	Be2	0.420	0.428	0.008
	Be3	0.413	0.534	0.121
	H1	0.000	-0.202	-0.202
	H2	0.000	-0.178	-0.178
P–BeONT	P	-0.419	-0.390	0.029
	Be1	0.574	0.584	0.010
	Be2	0.576	0.549	-0.027
	Be3	0.576	0.577	0.001
	H1	0.000	-0.012	-0.012
	H2	0.000	-0.009	-0.009
S–BeONT	S	-0.536	-0.502	0.034
	Be1	0.642	0.643	0.001
	Be2	0.643	0.643	0.000
	Be3	0.631	0.603	-0.028
	H1	0.000	0.002	0.002
	H2	0.000	-0.019	-0.019
Period 4:				
Ca–BeONT	Ca	1.142	1.159	0.017
	O1	-0.806	-0.803	0.003
	O2	-0.802	-0.802	0.000
	O3	-0.802	-0.809	-0.007
	H1	0.000	0.007	0.007

จุฬาลงกรณ์มหาวิทยาลัย
CHULALONGKORN UNIVERSITY

	H2	0.000	-0.029	-0.029
Ga–BeONT	Ga	0.673	0.728	0.055
	O1	-0.735	-0.735	0.000
	O2	-0.725	-0.726	-0.001
	O3	-0.725	-0.728	-0.003
	H1	0.000	-0.042	-0.042
	H2	0.000	-0.018	-0.018
$Ge^{(Be)}$–BeONT	Ge	0.682	0.707	0.025
	O1	-0.733	-0.736	-0.003
	O2	-0.734	-0.735	-0.001
	O3	-0.734	-0.735	-0.001
	H1	0.000	-0.028	-0.028
	H2	0.000	-0.007	-0.007
$Ge^{(O)}$–BeONT	Ge	-0.109	-0.076	0.033
	Be1	0.489	0.488	-0.001
	Be2	0.489	0.490	0.001
	Be3	0.483	0.472	-0.011
	H1	0.000	-0.023	-0.023
	H2	0.000	-0.021	-0.021
As–BeONT	As	-0.310	-0.284	0.026
	Be1	0.556	0.560	0.004
	Be2	0.554	0.556	0.002
	Be3	0.547	0.530	-0.017
	H1	0.000	-0.006	-0.006
	H2	0.000	-0.022	-0.022
Se–BeONT	Se	-0.462	-0.464	-0.002
	Be1	0.612	0.617	0.005
	Be2	0.612	0.617	0.005
	Be3	0.607	0.604	-0.003
	H1	0.000	0.010	0.010
	H2	0.000	-0.022	-0.022

[a] Atomic labels are shown in **Figure 4.11**; four atoms in rows (1–4) and two atoms in the last two rows possess the surface and hydrogen molecules, respectively.

[b] Change of Mülliken–charges of selected atom in specific surfaces, in e, compared with a clean surface.

จุฬาลงกรณ์มหาวิทยาลัย
Chulalongkorn University

4.3 Hydrogen absorption and sensing abilities of M-BeONTs comparing with other nanotubes in literature

The hydrogen adsorption abilities of pristine BeONTs is in order: (5,5) BeONT (ΔE_{ads}= –0.10 eV) > (10,0) BeONT (ΔE_{ads} = –0.08 eV) and their adsorption energies are quite as same as the BeONC (ΔE_{ads} = –0.11eV)[63] and BeOCs (BeO cluster) (ΔE_{ads} = –0.12 eV)[64] as shown in **Table 4.2**. Nevertheless, the (5,5) BeONT and (10,0) BeONT are opened-end nanotubes, but BeONC and BeOCs are closed-end nanotubes of which sizes are much smaller. The strongest hydrogen adsorption abilities of (5,5) BeONTs doped by elements in by elements in 2nd, 3rd and 4th period are $C^{(O)}$–BeONT (ΔE_{ads} = –4.73 eV), $Si^{(O)}$–BeONT (ΔE_{ads} = –2.92 eV) and $Ge^{(O)}$–BeONT (ΔE_{ads} = –1.96 eV), respectively. For the strongest hydrogen adsorption abilities of (10,0) BeONTs doped by elements in 2nd, 3rd and 4th period are $C^{(O)}$–BeONT (ΔE_{ads} = –4.75 eV), $Si^{(O)}$–BeONT (ΔE_{ads} = –2.56 eV) and Ca–BeONT (ΔE_{ads} = –0.19 eV), respectively. Adsorption abilities of hydrogen molecules on the $C^{(O)}$–(5,5) BeONT, $Si^{(O)}$–(5,5) BeONT, $Ge^{(O)}$–(5,5) BeONT, $C^{(O)}$–(10,0) BeONT and $Si^{(O)}$–(10,0) BeONT are much stronger than on the SWCNTs, of which adsorption energies are within the range from −0.034 to −0.035 eV (−0.78 to −0.81 kcal/mol)[66], the Ce/SWCNT (ΔE_{ads} = −0.16 to −0.33 eV/H_2)[5] , Ce/SWCNT (ΔE_{ads} = −0.22 to −0.49 eV/H_2)[4] and −0.33 and the Ce/BNNT (ΔE_{ads} = −0.28 eV/H_2)[22].

Chulalongkorn University

The outstanding changes in energy gap after hydrogen molecule adsorption of (5,5) BeONTs doped by elements in 2nd and 4th period are $C^{(O)}$–BeONT (ΔE_g=575.89%) and $Ge^{(O)}$–BeONT (ΔE_g=293.31%) and of (10,0) BeONTs doped by elements in by elements in 2nd, 3rd and 4th period are $C^{(O)}$–BeONT (ΔE_g=714.68%), $Si^{(O)}$–BeONT (ΔE_g=227.76%) and $Ge^{(O)}$–BeONT (ΔE_g=94.53%). Thus, the $C^{(O)}$– (5,5) BeONT, $Ge^{(O)}$– (5,5) BeONT, $Si^{(O)}$– (10,0) BeONT, $C^{(O)}$– (10,0) BeONT, and $Ge^{(O)}$– (10,0) BeONT are sensitive to their hydrogen molecule adsorption. If the recovery time in equation (3.5) was considered, the material with low adsorption ability with the enormous energy–gap change must be suggested as the excellent hydrogen

sensing material. Therefore, the $Ge^{(O)}$–BeONT was suggested as the best candidate to be a sensing material for hydrogen molecules.

จุฬาลงกรณ์มหาวิทยาลัย
Chulalongkorn University

CHAPTER V
CONCLUSION

The periodic DFT–D optimized structures of (5,5) and (10,0) BeONTs, and their surfaces doped by selected elements of periods 2 (B, C and N), 3 (Mg, Al, Si, P and S) and 4 (Ca, Ga, Ge, As and Se), were obtained. The strongest adsorptions of hydrogen molecule on the (5,5) BeONTs and (10,0) BeONTs, doped by periods 2, 3 and 4 element, are respectively the $C^{(O)}$–, $Si^{(O)}$– and $Ge^{(O)}$–doped (5,5) BeONTs, and $C^{(O)}$–, $Si^{(O)}$– and Ca–doped (10,0) BeONTs. The strengths of hydrogen molecule on the $C^{(O)}$–, $Si^{(O)}$– and $Ge^{(O)}$–doped (5,5) BeONTs, and $C^{(O)}$–, $Si^{(O)}$– and Ca–doped (10,0) BeONTs, are in orders: $C^{(O)}$ (ΔE_{ads}= –4.73 eV) > $Si^{(O)}$ (ΔE_{ads}= –2.92 eV) > $Ge^{(O)}$ (ΔE_{ads}= –1.96 eV), and the $C^{(O)}$ (ΔE_{ads}= –4.75 eV) > $Si^{(O)}$ (ΔE_{ads}= –2.56 eV) > Ca (ΔE_{ads}= –0.19 eV), respectively. The largest values of energy–gap change after adsorbing hydrogen molecule of the (5,5) and (10,0) BeONTs, doped by periods 2, 3 and 4 element, are $C^{(O)}$– (ΔE_g= 575.89%), Mg– (ΔE_g= 4.23%) and $Ge^{(O)}$– (ΔE_g= 293.31%), and $C^{(O)}$– (ΔE_g= 714.68%), $Si^{(O)}$– (ΔE_g= 227.76%) and $Ge^{(O)}$– (ΔE_g= 94.53%), respectively. Therefore, the $C^{(O)}$– and $Ge^{(O)}$–(5,5) BeONTs, $C^{(O)}$–, $Si^{(O)}$– and $Ge^{(O)}$–(10,0) BeONTs can to be new sensing materials for hydrogen molecule and the $Ge^{(O)}$–(10,0) BeONT was suggested to be utilized as excellent hydrogen molecule sensing material based on the electrical resistivity measurement. The $C^{(O)}$–, $Si^{(O)}$– and $Ge^{(O)}$–doped (5,5) BeONTs, and $C^{(O)}$– and $Si^{(O)}$–doped (10,0) BeONTs were suggested to be utilized as hydrogen storage materials.

APPENDICES

Table S1 The GRIMME, D2 parameters of the London-type empirical correction for dispersion interactions of all the elements used in this work

Elements	C_6 [a]	R_{vdw} [b]
s6 = 0.75 [c], d= 20.0 [d], R_{cut} = 25.0 [e]		
Nanotubes:		
Be	1.61	1.408
O	0.70	1.342
Dopants:		
Period 2		
B	3.13	1.485
C	1.75	1.452
N	1.23	1.397
Period 3		
Mg	5.71	1.364
Al	10.79	1.716
Si	9.23	1.716
P	7.84	1.705
S	5.57	1.683
Period 4		
Ca	10.80	1.474
Ga	16.99	1.650
Ge	17.10	1.727
As	16.37	1.760
Se	12.64	1.771
Adsorbate:		
H	0.14	1.001

[a] dispersion coefficient for atom in J nm^6 mol^{-1}.

[b] Van der Waals radius for atom, in Å.

[c] Scaling factor.

[d] Steepness.

[e] Cutoff distance to truncate direct lattice summation.

จุฬาลงกรณ์มหาวิทยาลัย
Chulalongkorn University

P1	H																He
P2	Li	Be											B	C	N	O	F	Ne
P3	Na	Mg											Al	Si	P	S	Cl	Ar
P4	K	Ca	Sc	Ti	V	Cr	Mn	Fe	Co	Ni	Cu	Zn	Ga	Ge	As	Se	Br	Kr

Figure S1 The elements used in this work are on the black-ground colors, shown as the periodic-based TABLE. Blue, pink, and red colors are non-metal, metalloid and metal elements, respectively. The atoms highlighted in red were positioned as the middle atoms within electron-deficient (B, Al, and Ga) and electron-rich (N, P and As) atoms. The P1, P2, P3, and P4 are the periods 1, 2, 3, and 4, respectively

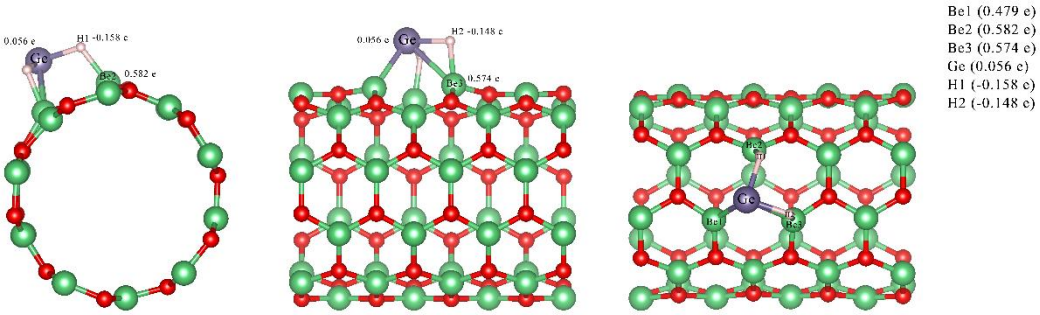

CHULALONGKORN UNIVERSITY

Figure S2 Adsorption structures of H_2 adsorbed on the $Ge^{(O)}$–(5,5) BeONTs to form hydrogen-bridged structure. Left, middle and right images are front, side, and top views, respectively. The atomic charges are shown in parentheses

REFERENCES

จุฬาลงกรณ์มหาวิทยาลัย
Chulalongkorn University

REFERENCES

[1] S. Iijima, Helical microtubules of graphitic carbon, Nature, 354 (1991) 56-58.

[2] A. Zolfaghari, F. Hashemi, P. Pourhossein, H. Jooya, Molecular dynamics simulations on the effect of temperature and loading in H_2 exohedral adsorption on (3,3) and (9,9) SWCNTs, International Journal of Hydrogen Energy, 32 (2007) 4889-4893.

[3] S. Ghosh, V. Padmanabhan, Adsorption of hydrogen on single-walled carbon nanotubes with defects, Diamond and Related Materials, 59 (2015) 47-53.

[4] Z.W. Zhang, J.C. Li, Q. Jiang, Hydrogen Adsorption on Eu/SWCNT Systems: A DFT Study, The Journal of Physical Chemistry C, 114 (2010) 7733-7737.

[5] Z. Zhang, W. Zheng, Q. Jiang, Hydrogen adsorption on Ce/SWCNT systems: a DFT study, Physical chemistry chemical physics : PCCP, 13 (2011) 9483-9489.

[6] B.J. Nagare, D. Habale, S. Chacko, S. Ghosh, Hydrogen adsorption on Na–SWCNT systems, Journal of Materials Chemistry, 22 (2012) 22013-22021.

[7] A.S. Shalabi, S. Abdelaal, M.M. Assem, W. Abdel Halim, Ab initio characterization of Ti decorated SWCNT for hydrogen storage, International Journal of Hydrogen Energy, 38 (2013) 140–152.

[8] A. Shalabi, A. Mahdy, H. Taha, Theoretical characterization of axial deformation effects on hydrogen storage of Ti decorated armchair (5,5) SWCNT, Molecular Physics, 111 (2013) 661-671.

[9] D.S. Niaz, H. Abbasian, M. Badar, a.-u.-h. Muhammad, A. Karayel, Theoretical study of hydrogen adsorption in Ti-decorated capped carbon nanotube, Molecular Physics, 115 (2017) 1-6.

[10] C. Kaewkhonkaen, V. Ruangpornvisuti, Hydrogen adsorption on Pt-decorated closed-end armchair (3,3), (4,4) and (5,5) single-walled carbon nanotubes, Molecular Physics, 114 (2016) 1-10.

[11] R. Ma, Y. Bando, H. Zhu, T. Sato, C. Xu, D. Wu, Hydrogen Uptake in Boron Nitride Nanotubes at Room Temperature, J. Am. Chem. Soc., 124 (2002) 7672-7673.

[12] S.-H. Jhi, Y.-K. Kwon, Hydrogen adsorption on boron nitride nanotubes: A path to room-temperature hydrogen storage, Physical Review B, 69 (2004) 245407.

[13] X. Wu, J. Yang, J.G. Hou, Q. Zhu, Hydrogen adsorption on zigzag (8,0) boron nitride nanotubes, The Journal of Chemical Physics, 121 (2004) 8481-8485.

[14] X. Wu, J. Yang, J. Hou, Q. Zhu, Deformation-induced site selectivity for hydrogen adsorption on boron nitride nanotubes, Physical Review B, 69 (2004) 153411.

[15] S.S. Han, J. Kang, H. Lee, A. van Duin, W. Goddard, Theoretical study on interaction of hydrogen with single-walled boron nitride nanotubes. II. Collision, storage, and adsorption, The Journal of chemical physics, 123 (2005) 114704.

[16] L. Xiu-Ying, W. Chao-Yang, T. Yong-Jian, S. Wei-Guo, W. Wei-Dong, X. Jia-Jing, Theoretical studies on hydrogen adsorption of single-walled boron-nitride and carbon nanotubes using grand canonical Monte Carlo method, Physica B: Condensed Matter, 404 (2009) 1892-1896.

[17] Z. Zhou, J. Zhao, Z. Chen, X. Gao, T. Yan, B. Wen, P.v.R. Schleyer, Comparative Study of Hydrogen Adsorption on Carbon and BN Nanotubes, The Journal of Physical Chemistry B, 110 (2006) 13363-13369.

[18] X. Wu, J. Yang, J.G. Hou, Q. Zhu, Defects-enhanced dissociation of H_2 on boron nitride nanotubes, The Journal of Chemical Physics, 124 (2006) 054706.
[19] R. Baierle, P. Piquini, T. Schmidt, A. Fazzio, Hydrogen Adsorption on Carbon-Doped Boron Nitride Nanotube, The journal of physical chemistry. B, 110 (2006) 21184-21188.
[20] X. Wu, J. Yang, X. Chen, Adsorption of hydrogen molecules on the platinum-doped boron nitride nanotubes, The Journal of chemical physics, 125 (2006) 44704.
[21] M. Noura, A. Rahdar, S.M. Taimoory, J.J. Hayward, S.I. Sadraei, J.F. Trant, A theoretical first principles computational investigation into the potential of aluminum-doped boron nitride nanotubes for hydrogen storage, International Journal of Hydrogen Energy, 45 (2020) 11176-11189.
[22] Z.-W. Zhang, W.-T. Zheng, Q. Jiang, Hydrogen adsorption on Ce/BNNT systems: A DFT study, International Journal of Hydrogen Energy, 37 (2012) 5090-5099.
[23] L.P. Zhang, P. Wu, M.B. Sullivan, Hydrogen Adsorption on Rh, Ni, and Pd Functionalized Single-Walled Boron Nitride Nanotubes, The Journal of Physical Chemistry C, 115 (2011) 4289-4296.
[24] M. Mananghaya, G.N. Santos, D. Yu, Hydrogen adsorption of Ti-decorated boron nitride nanotube: a density functional based tight binding molecular dynamics study, Adsorption, 24 (2018).
[25] M.R. Mananghaya, Titanium-decorated boron nitride nanotubes for hydrogen storage: a multiscale theoretical investigation, Nanoscale, 11 (2019) 16052-16062.
[26] M. Mananghaya, A simulation of hydrogen adsorption/desorption in metal-functionalized BN nanotube, Materials Chemistry and Physics, 240 (2019) 122159.
[27] P.B. Sorokin, A.S. Fedorov, L.A. Chernozatonskiĭ, Structure and properties of BeO nanotubes, Physics of the Solid State, 48 (2006) 398-401.
[28] B. Baumeier, P. Krüger, J. Pollmann, Structural, elastic, and electronic properties of SiC, BN, and BeO nanotubes, Physical Review B, 76 (2007) 085407.
[29] M. Gorbunova, I. Shein, Y. Makurin, V. Ivanovskaya, V. Kijko, A. Ivanovskii, Electronic structure and magnetism in BeO nanotubes induced by boron, carbon and nitrogen doping, and beryllium and oxygen vacancies inside tube walls, Physica E-low-dimensional Systems & Nanostructures - PHYSICA E, 41 (2008) 164-168.
[30] J. He, K. Wu, R. Sa, Q. Li, Y. Wei, Modulating the electronic structures and optical absorption spectra of BeO nanotubes by uniaxial strain, Applied Physics Letters, 97 (2010) 051901.
[31] A. Fathalian, R. Moradian, M. Shahrokhi, Optical properties of BeO nanotubes: Ab initio study, Solid State Communications, 156 (2013) 1–7.
[32] J.-M. Zhang, H.-H. Li, Y. Zhang, K.-W. Xu, Structural, electronic and magnetic properties of the 3d transition-metal-doped AlN nanotubes, Physica E-low-dimensional Systems & Nanostructures - PHYSICA E, 43 (2011) 1249-1254.
[33] M. Sabzehzari, T. Ahmadi, H. Bahrami, Effect of B, Al and Ga atoms on structures, electrical and optical properties of BeO nanotube, ChemistrySelect, 4 (2019) 6739-6743.
[34] B. Arghavani Nia, M. Shahrokhi, Dilute magnetic semiconductor and half-metal behaviors in C-codoped BeO nanotubes: A first principles simulations, Chinese Journal of Physics, 56 (2018).

[35] S. Xu, W. Liu, Z. Zhu, C. Li, G. Yuan, Electronic structure and field emission characteristics of a new kind of BeO nanotubes: A first-principles study, Journal of Vacuum Science & Technology B, 39 (2021) 030601.
[36] N. Ahmadaghaei, M. Noei, Density functional study on the sensing properties of nano-sized BeO tube toward H_2S, Journal of the Iranian Chemical Society, 11 (2013).
[37] M. Kamani, A.A. Salari, M. Noei, N. Ahmadaghaei, S. Mohajeri, M. Ebrahimikia, N. Molaei, Adsorption of Aniline Toxic Gas on a BeO Nanotube, IRANIAN JOURNAL OF CHEMISTRY & CHEMICAL ENGINEERING-INTERNATIONAL ENGLISH EDITION, 38 (2019) 43-48.
[38] M. Nayebzadeh, H. Soleymanabadi, Z. Bagheri, Adsorption and dissociation of nitrous oxide on pristine and defective BeO and ZnO nanotubes: DFT studies, Monatshefte für Chemie - Chemical Monthly, 145 (2014).
[39] A. Ahmadi Peyghan, S. Yourdkhani, Capture of carbon dioxide by a nanosized tube of BeO: A DFT study, Structural Chemistry, 25 (2014).
[40] M. Sherafati, A. Shokuhi Rad, M. Ardjmand, A. Heydarinasab, M. Peyravi, M. Mirzaei, Beryllium oxide (BeO) nanotube provides excellent surface towards adenine adsorption: A dispersion-corrected DFT study in gas and water phases, Current Applied Physics, 18 (2018) 1059-1065.
[41] J. Baima, A. Erba, M. Rérat, R. Orlando, R. Dovesi, Beryllium oxide nanotubes and their connection to the flat monolayer, J. Phys. Chem. C, 117 (2013) 12864-12872.
[42] J. he, K. Wu, R. sa, L. Qiaohong, Y. Wei, Modulating the electronic structures and optical absorption spectra of BeO nanotubes by uniaxial strain, Applied Physics Letters, 97 (2010) 051901-051901.
[43] H. Rezania, Z. Manesh, Electronic Correlation Effects on the Optical Properties of SiC, BeO and Boron Nitride Nanotubes and Monolayers, Communications in Theoretical Physics, 64 (2015) 583-589.
[44] M. Sabzehzari, T. Ahmadi, H. Bahrami, Effect of B, Al and Ga atoms on structures, electrical and optical properties of BeO nanotube, 4 (2019) 6739-6743.
[45] A. Seif, E. Zahedi, G.M. Rozbahani, A computational investigation of carbon-doped beryllium monoxide nanotubes, Central European Journal of Chemistry, 10 (2012) 96-104.
[46] W. Yu, Z. Zhu, C.-Y. Niu, C. Li, J.-H. Cho, Y. Jia, Dilute Magnetic Semiconductor and Half-Metal Behaviors in 3d Transition-Metal Doped Black and Blue Phosphorenes: A First-Principles Study, Nanoscale Research Letters, 11 (2016) 77.
[47] M.A. Gorbunova, I.R. Shein, Y.N. Makurin, V.V. Ivanovskaya, V.S. Kijko, A.L. Ivanovskii, Electronic structure and magnetism in BeO nanotubes induced by boron, carbon and nitrogen doping, and beryllium and oxygen vacancies inside tube walls, Physica E Low-Dimensional Systems and Nanostructures, 41 (2008) 164-168.
[48] J.M. Zhang, W.T. Song, H.H. Li, K.W. Xu, J. Vincent, Effects of the 3d transition metal doping on the structural, electronic, and magnetic properties of BeO nanotubes, Chinese Physics B, 23 (2014).
[49] J. Beheshtian, I. Ravaei, Hydrogen storage by BeO nano-cage: A DFT study, Applied Surface Science, 368 (2016) 76-81.

[50] A. Lichanot, M. Chaillet, C. Larrieu, R. Dovesi, C. Pisani, Ab initio Hartree-Fock study of solid beryllium oxide: structure and electronic properties, Chemical Physics, 164 (1992) 383-394.
[51] A.L. Ivanovskii, I.R. Shein, Y.N. Makurin, V.S. Kiiko, M.A. Gorbunova, Electronic structure and properties of beryllium oxide, Inorganic Materials, 45 (2009) 223-234.
[52] S. Duman, A. Sütlü, S. Bağcı, H.M. Tütüncü, G.P. Srivastava, Structural, elastic, electronic, and phonon properties of zinc-blende and wurtzite BeO, Journal of Applied Physics, 105 (2009).
[53] B. Baumeier, P. Krüger, J. Pollmann, Structural, elastic, and electronic properties of SiC, BN, and BeO nanotubes, Physical Review B, 76 (2007).
[54] S.M. Blinder, Chapter 14 - Density functional theory, in: S.M. Blinder (Ed.) Introduction to Quantum Mechanics (Second Edition), Academic Press, San Diego, 2021, pp. 235-244.
[55] R. Dovesi, R. Orlando, A. Erba, C.M. Zicovich-Wilson, B. Civalleri, S. Casassa, L. Maschio, M. Ferrabone, M. De La Pierre, P. D'Arco, Y. Noël, M. Causà, M. Rérat, B. Kirtman, CRYSTAL14: A program for the ab initio investigation of crystalline solids, International Journal of Quantum Chemistry, 114 (2014) 1287-1317.
[56] S. Grimme, Semiempirical GGA-type density functional constructed with a long-range dispersion correction, J. Comput. Chem., 27 (2006) 1787-1799.
[57] J.P. Perdew, K. Burke, M. Ernzerhof, Generalized Gradient Approximation Made Simple, Physical Review Letters, 77 (1996) 3865-3868.
[58] R. Dovesi, A. Erba, R. Orlando, C.M. Zicovich-Wilson, B. Civalleri, L. Maschio, M. Rérat, S. Casassa, J. Baima, S. Salustro, B. Kirtman, Quantum-mechanical condensed matter simulations with CRYSTAL, WIREs Computational Molecular Science, 8 (2018) e1360.
[59] J. Heyd, J.E. Peralta, G.E. Scuseria, R.L. Martin, Energy band gaps and lattice parameters evaluated with the Heyd-Scuseria-Ernzerhof screened hybrid functional, The Journal of Chemical Physics, 123 (2005) 174101.
[60] R. Dovesi, C. Ermondi, E. Ferrero, C. Pisani, C. Roetti, Hartree-Fock study of lithium hydride with the use of a polarizable basis set, Physical Review B, 29 (1984) 3591-3600.
[61] K. Momma, F. Izumi, VESTA 3 for three-dimensional visualization of crystal, volumetric and morphology data, Journal of Applied Crystallography, 44 (2011) 1272-1276.
[62] S. Peng, K. Cho, P. Qi, H. Dai, Ab initio study of CNT NO_2 gas sensor, Chem. Phys. Lett., 387 (2004) 271-276.
[63] J. Beheshtian, I. Ravaei, Hydrogen storage by BeO nano-cage: A DFT study, Applied Surface Science, 368 (2016).
[64] R. Shinde, M. Tayade, Remarkable Hydrogen Storage on Beryllium Oxide Clusters: First-Principles Calculations, The Journal of Physical Chemistry C, 118 (2014) 17200-17204.
[65] J. Baima, A. Erba, M. Rérat, R. Orlando, R. Dovesi, Beryllium Oxide Nanotubes and their Connection to the Flat Monolayer, The Journal of Physical Chemistry C, 117 (2013) 12864-12872.

[66] I.K. Petrushenko, K.B. Petrushenko, Physical adsorption of hydrogen molecules on single-walled carbon nanotubes and carbon-boron-nitrogen heteronanotubes: A comparative DFT study, Vacuum, 167 (2019) 280-286.

จุฬาลงกรณ์มหาวิทยาลัย
Chulalongkorn University

VITA

NAME	kritsanaphas sawing
DATE OF BIRTH	6 July 1992
PLACE OF BIRTH	Thailand
INSTITUTIONS ATTENDED	M.Sc. in Chemistry, Chulalongkorn University B.Sc. in Chemistry, Chulalongkorn University
HOME ADDRESS	125/3 Chor Hae Road, Nai Wiang, Mueang Phrae District, Phrae 54000
PUBLICATION	Sawing, K.; Ruangpornvisuti, V., Hydrogen molecule adsorption on pristine and selected-elements (periods 2-4)-doped armchair (5,5) and zigzag (10,0) beryllium oxide nanotubes as hydrogen storage materials. International Journal of Energy Research 2021.

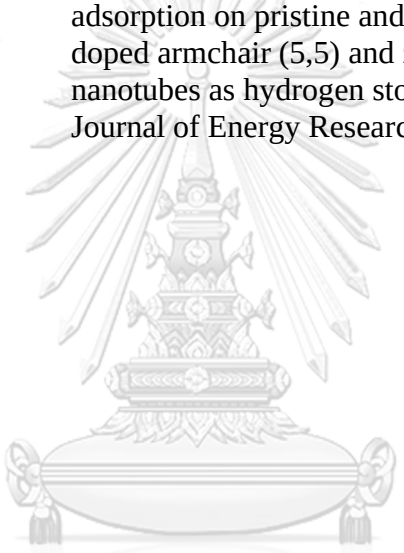

จุฬาลงกรณ์มหาวิทยาลัย
Chulalongkorn University